3D Numerical modelling of a voice-producing element

Manon Hegeman

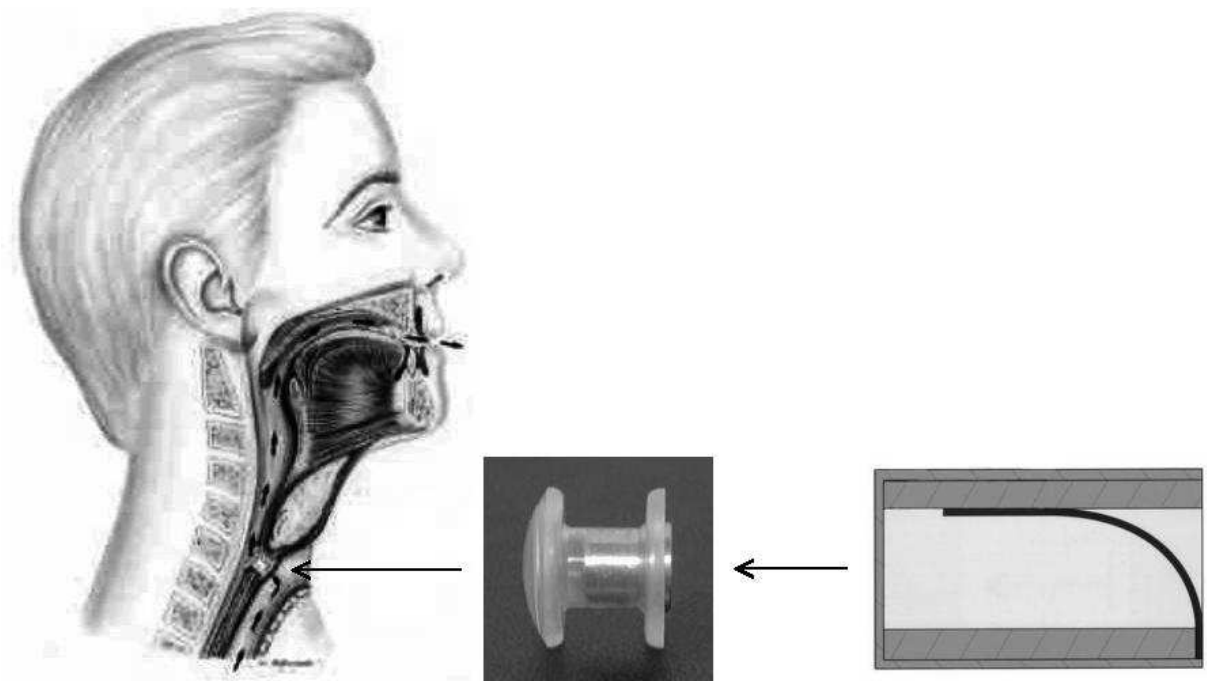

Department of Mathematics

RuG

Master's Thesis

3D Numerical modelling of a voice-producing element

Manon Hegeman

Supervisor:
Prof.dr. A.E.P. Veldman
Department of Mathematics
University of Groningen
P.O. Box 800
9700 AV Groningen

May 2004

Contents

List of symbols **3**

Introduction **5**

1 Laryngectomy **7**
1.1 Alaryngeal voice . . . 7
1.1.1 Electrolaryngeal voice . . . 7
1.1.2 Injection esophageal voice . . . 8
1.1.3 Tracheo-esophageal voice . . . 9
1.2 Voice-producing element . . . 10
1.2.1 In vitro and in vivo experiments . . . 11

2 Development of the computational model **13**
2.1 Two-dimensional computational model . . . 13
2.1.1 The vocal tract, the subglottal tract and the shunt valve . . . 15
2.2 Three-dimensional computational model . . . 16
2.3 Numerical solution algorithm . . . 17

3 Detailed computational model **19**
3.1 The fluid . . . 19
3.1.1 Computational grid . . . 19
3.1.2 Discretization in time . . . 20
3.1.3 Discretization in space . . . 20
3.1.4 Solution method . . . 21
3.2 The structure . . . 21
3.2.1 Discretization in space . . . 21
3.2.2 Solution method . . . 22
3.3 The grid . . . 23
3.4 The flow of information . . . 23
3.5 Data . . . 24

4 Verification **25**
4.1 Compiler . . . 26
4.2 Epsilon . . . 28
4.3 Courant-Friedrichs-Levy number . . . 28
4.4 Grid research . . . 31
4.5 Conclusions . . . 35

5 Parameter study **37**
5.1 Damping coefficients . . . 37
5.1.1 c_{mass} . . . 37
5.1.2 c_{stiff} . . . 38
5.2 Elasticity modulus . . . 40
5.3 Pressure . . . 41
5.4 Number of dimensions . . . 43
5.4.1 Necessity of a 3D computational model . . . 43
5.5 Conclusions . . . 46

6 Validation **49**
6.1 In vitro experiments . . . 49
6.2 Earlier results . . . 51

7 Conclusions **53**
7.1 Future work . . . 54
7.1.1 Numerical adjustments . . . 54
7.1.2 Physical adjustments . . . 55
7.1.3 Lower priority adjustments . . . 56

A Coupled problems **59**
A.1 Classification of coupled problems . . . 59
A.1.1 Strong and weak . . . 59
A.1.2 Extent . . . 59
A.1.3 Discretization method . . . 60
A.1.4 Global non-linear numerical solution algorithm . . . 60
A.2 Solving coupled problems . . . 60
A.2.1 Monolithic and partitioned coupling scheme . . . 60
A.2.2 Parameter and geometry coupling . . . 62
A.2.3 Block Jacobi and block Gauss-Seidel scheme . . . 62
A.2.4 Loose coupling and predictor-corrector algorithm . . . 62

Bibliography **67**

List of symbols

c_{mass}	dampingscoefficient $\frac{1}{s}$
c_{stiff}	dampingscoefficient s
E	elasticity modulus $Pa \quad (= \frac{kg}{m\ s^2})$
$\boldsymbol{F}$	force vector $N \quad (= \frac{kg\ m}{s^2})$
$F0$	fundamental frequency Hz
M	moment $N\ m \quad (= \frac{kg\ m^2}{s^2})$
p	pressure $Pa \quad (= \frac{kg}{m\ s^2})$
Q	flow $\frac{m^3}{s}$
SPL	sound pressure level dB
t	time s
$\boldsymbol{u}$	velocity vector $\frac{m}{s}$

$\boldsymbol{V}$	vector containing:	
	u	horizontal displacement
		m
	v	vertical displacement
		m
	ϕ	rotation
		$radians$
x	axial coordinate	
	m	
y	lateral coordinate	
	m	
z	vertical coordinate	
	m	
ν	kinematic viscosity (with $\nu_{air} = 1.33 \cdot 10^{-5}\ \frac{m^2}{s}$)	
	$\frac{m^2}{s}$	
ρ	density (with $\rho_{air} = 1.2\ \frac{kg}{m^3}$)	
	$\frac{kg}{m^3}$	

Introduction

During speech and singing, people make sound by using their vocal folds, which are located in the larynx. When exhaling, air passes the vocal folds. This interaction causes the vocal folds to vibrate, by which vibrating air is created, which is later converted to the sounds we hear in speech and singing. If these vocal folds are removed by a surgical procedure, such as a total laryngectomy, the natural way of voice production, laryngeal voice, is no longer possible (figure 1) [27].

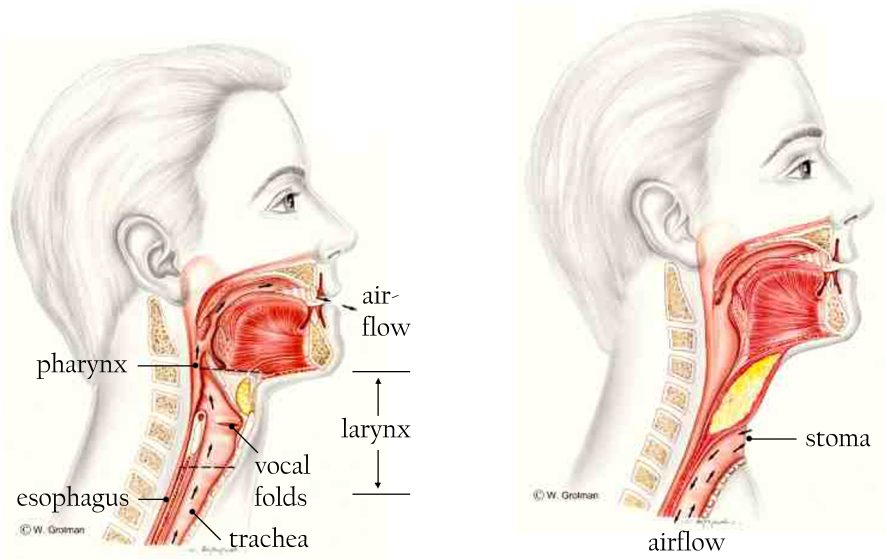

Figure 1: Before a laryngectomy (left) and after a total laryngectomy (right)

To restore audible speech (with a tracheo-esophageal voice) after a laryngectomy, a voice-producing element has been developed. This device consists of a flexible lip of silicone rubber placed in a metal housing, which is placed in a shunt valve (figure 2).

The voice-producing element has already been tested in in vitro and in vivo experiments. From these experiments it turned out that the voice-producing element still has some deficiencies. Numerical experiments might be very useful to improve the behavior of the voice-producing element.

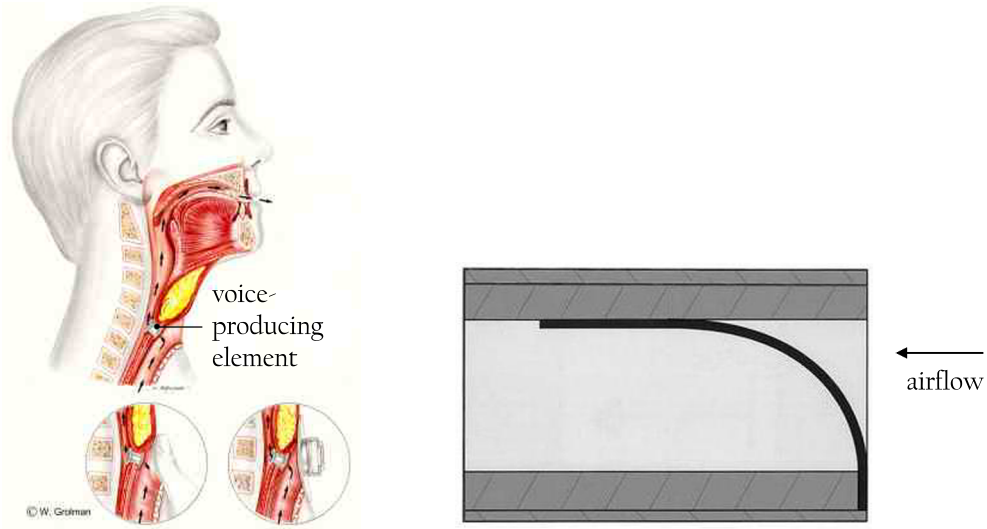

Figure 2: Tracheo-esophageal voice (left) and a schematic representation of a voice-producing element (right)

At the moment there already exist two-dimensional numerical models. However, there are several disadvantages of a two-dimensional numerical model, because this model contains no width. For example, no air is allowed to flow along the sides of the lip and no torsion of the lip is possible. These disadvantages can be solved by developing a three-dimensional numerical model, where the third dimension represents the width of the lip.

In this thesis we will first enlarge upon the surgical procedure of a laryngectomy and the usage of a voice-producing element in chapter 1. Second, attention will be paid to the development of a computational model of a voice-producing element in chapter 2 and in chapter 3 the developed computational model will be analyzed in more detail. After the development of the computational model, the results obtained with this model will be verified in chapter 4. In chapter 5 more investigation of these obtained results will be done by a parameter study and the necessity of a three-dimensional numerical model will be examined. In chapter 6 the results will be validated. Finally, the conclusions and future work about the developed computational model and the obtained results are presented in chapter 7.

Chapter 1

Laryngectomy

The surgical procedure of a laryngectomy is most often carried out as a treatment for cancer of the larynx. There are two types of laryngectomy [3]. A partial laryngectomy is possible if a tumour is small. With this procedure only a part of the larynx, for example one vocal fold, is removed, which means that the voice is not fully lost. In a total laryngectomy the entire larynx, i.e. including both vocal folds, is removed, so that natural sound generation is no longer possible. The upper part of the trachea is lead to a permanent opening in the front of the neck, called a tracheostoma or simply stoma, so that the esophagus and the trachea are completely separated. Consequently, airflow from the lungs can no longer pass the mouth and nose. The esophagus, however, is usually not affected and is still connected to the pharynx [3, 27].

1.1 Alaryngeal voice

There are three main types of voice production possible after a laryngectomy, called alaryngeal voice [3, 15, 18, 23, 27]:

- electrolaryngeal voice;
- injection esophageal voice;
- tracheo-esophageal voice.

1.1.1 Electrolaryngeal voice

In electrolaryngeal voice (figure 1.1) the patients, called laryngectomees, make use of an electrolarynx, an electro-mechanical hand-held device that produces vibrations. If the device is held to the right spot on the neck it causes vibrations in the throat, so that voiced speech is possible.

The main disadvantage of an electrolarynx is the mechanical and monotonous tone during speech that does not sound natural. The advantages of speaking with an electrolarynx are the ability of learning it in a short time and the production of a respectively loud voice. Furthermore, most devices have functions that can set the fundamental frequency of the vibrations, depending on the age and gender of the speaker [15, 18, 27]. The mean fundamental frequency ($F0$) of laryngeal voice, is 210 Hz for women and 110 Hz for men [18, 23].

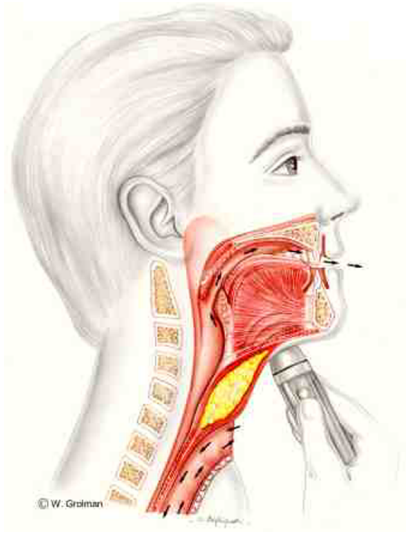

Figure 1.1: Electrolaryngeal voice

1.1.2 Injection esophageal voice

In general, injection esophageal voice (figure 1.2) is simply called esophageal voice. It is produced when air is "swallowed", i.e. injected in the esophagus, and escapes in a controlled fashion, so that vibrations arise in the esophagus entrance and in the pharynx and generation of sounds is possible. It is difficult and may take a long time to learn how to use an esophageal voice. Other disadvantages are the rough sound and the difficulty of speaking long sentences without taking breaks to bring in more air [18, 27]. But the advantage of esophageal voice are the small costs, compared to the other substitute voice methods [15].

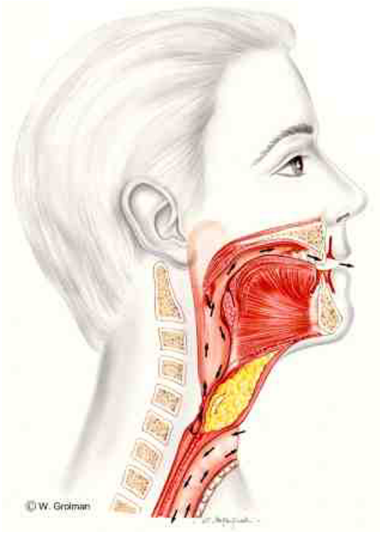

Figure 1.2: Injection esophageal voice

Different $F0$ of esophageal voice are found. Mitchell and Moretz [23] mention a range from 60 to 80 Hz. De Vries [8] cites a range from 60 to 90 Hz. Van der Torn et al. [33] mention

a range from 60 to 120 Hz. Finally Hočevar-Boltežar and Žargi [18] found results that range from 57 to 136 Hz, which usually are lower than the average laryngeal $F0$. The conclusion of all these findings is that esophageal voice might be acceptable for men, but simply gives a too low voice for women.

1.1.3 Tracheo-esophageal voice

The last type of voice, tracheo-esophageal voice (TE voice), is also the most effective one. It resembles injection esophageal voice, except that TE voice uses a different source for the air.

With TE voice (figure 1.3) a small opening, called a shunt, fistula or tracheoesophageal puncture, is created in the esophageal wall and a small one-way shunt valve, usually called a voice prosthesis (although this device does not actually produce sound) is placed into the shunt so that the trachea and the esophagus are connected. The TE shunt valve makes sure no fluid or food enters the trachea and causes lung problems. In order to speak, the stoma has to be occluded during exhalation, so that the airflow from the lungs goes via the trachea and the shunt valve into the esophagus where it interacts with the esophageal wall and causes vibrating air. These sounds produced by the vibrating air are converted by adjustments made by the lips, tongue and jaw opening into speech. Occlusion of the stoma can be done by hand or by a tracheostoma valve. The latter is a device placed in the tracheostoma to control the air passage and allows hands free operation of the stoma [12].

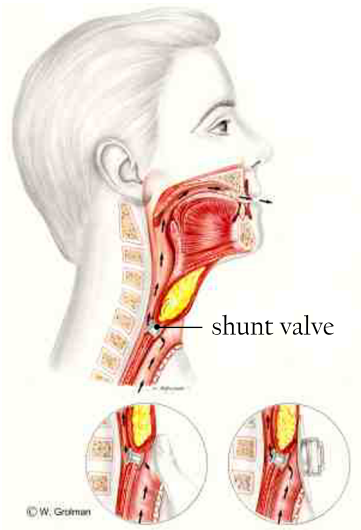

Figure 1.3: Tracheo-esophageal voice (Left: occlusion by hand. Right: occlusion by a tracheostoma valve.)

Advantages of TE voice [15, 18, 27]:

- The voice quality is relatively good compared to the other voice rehabilitation techniques. It most closely resembles normal laryngeal voice, although the frequencies do not differ much from the frequencies of the injection esophageal voice.
- Since the air for speaking comes from the lungs, one can speak for a considerably long time without breaks.

However, there are also a lot of disadvantages [15, 18, 27]:

- The $F0$ might be acceptable for men, but is still too low for women.
- Not everyone can use TE voice. In some cases the walls of the esophagus are too tight to vibrate.
- The shunt valve must be removed and cleaned periodically. This requires a moderate amount of proficiency, especially in putting it back in the right spot.
- The stoma must be tightly covered during exhalation in order to get air into the esophagus. This requires good arm and hand movement. Tracheostoma valves (lower right image in figure 1.3) exist that can be placed over the stoma to control the air passage into the esophagus, but they do not always work in daily practice and they are difficult to adhere to the skin.
- Fluid or food may leak into the trachea.
- Occasionally the prosthesis can fall out and the shunt will close in about 24 hours. If it does get closed, a second operation must be done to make a new shunt.

The $F0$ of TE voice is the same or a little higher than the $F0$ for esophageal voice. De Vries [8] mentions a $F0$ of 60 - 90 Hz. Searl and Small [31] establish a $F0$ of 154 Hz for women and 94 Hz for men. The $F0$ found by Hočevar-Boltežar and Žargi [18] ranges from 72 Hz to 134 Hz, but unfortunately these $F0$ are still too low for women.

Of these three substitute voice methods, TE voice is currently the option most often used after a laryngectomy, since it is the best. For instance, the sound quality of TE voice is relatively good, in contrast with electrolaryngeal voice, which has a very mechanical sound. The second reason for the better quality of TE voice is based on the fact that air comes from the lungs, while with injection esophageal voice air is injected and therefore returns from the esophagus. Since the esophagus has a smaller volume, the speech segments with injection esophageal voice are usually shorter. Finally with TE voice there is better control of the airflow [27].

1.2 Voice-producing element

To improve speech quality after a laryngectomy an artificial vocal fold is developed and placed in a TE shunt valve [8, 14, 16, 33, 34]. This device is called a voice-producing element (vpe) and is depicted in figure 1.4. It consists of a flexible lip of silicone rubber, which is placed in a rectangular hole in a cylindrical metal housing (figure 1.5). In the initial situation the lip is in neutral position, i.e. the lip is pressed against the wall opposite to the wall where the lip is inserted. When airflow passes the lip, the lip starts to vibrate and produces sound. This idea of a flexible lip is derived from the vibrating lips of a musician playing a brass instrument, but instead of a vpe consisting of 2 lips, the current vpe has a single lip, mainly because it is easier to fabricate [8, 34].

The $F0$ of the vpe depends on the geometry and material properties of the lip. For example, a longer lip produces a sound with a lower frequency. Thus by changing the geometry or material different $F0$ can be achieved [8, 16, 34].

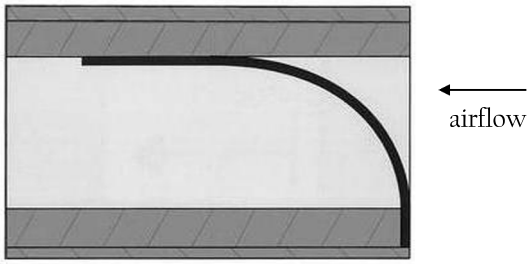

Figure 1.4: A schematic representation of a cross-section of a voice-producing element

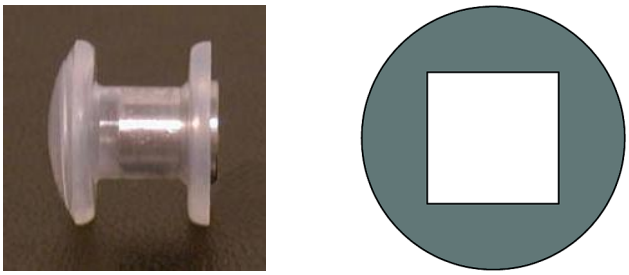

Figure 1.5: A picture of a voice-producing element placed in a shunt valve (airflow from the right) and a schematic representation of the front view of a voice-producing element (airflow from the front)

With the developing of a vpe there are several requirements concerning the sound [8, 34]:

- $F0$ of about 110 Hz for males and about 210 Hz for females;
- sound pressure level between 65 dB and 80 dB, measured at 30 cm distance from the mouth;
- sound pressure level variation of 5 - 10 dB [38];
- frequency variation of about 3 - 4 semitones (like a normal intonation pattern);
- flow as in normal voice production, between 0.18 and 0.32 L/s;
- pressure as in normal voice production, between 0.4 and 1.5 kPa.

1.2.1 In vitro and in vivo experiments

Several vpe's have already been tested in in vitro and in vivo experiments. Unfortunately not all requirements are met, but the results are acceptable [8, 34]. The required $F0$ for females (210 Hz) is realized, but the required $F0$ for males (110 Hz) is still not reached. The sound pressure level (SPL) rises with increasing flow, nevertheless it is still a little too low. As for the frequency variation, at least 3 semitones are gained, which is sufficient, but the change of frequency per pressure change is a little low.

Furthermore, it has to be taken into account that the lungs provide the flow and pressure for the vpe, meaning that the flow and pressure ranges must occur as in normal voice production.

Fortunately, the prototypes tested all operate within the limits set by the physical capabilities of the laryngectomees.

A disadvantage of the vpe is the established U-shaped relation between the $F0$ and the flow [8, 33, 34], i.e. an unexpected decrease of the frequency of the vpe by increasing flow, but when the flow is increased further the frequency rises again. This phenomenon is also seen during in vivo experiments of a vpe inserted in a shunt valve by laryngectomees [33]. An explanation might be the variance of the modes of vibration of the silicone rubber lip at specific flow levels, i.e. at some flow levels the lip starts to vibrate differently [29].

Finally, it has to be mentioned that during the in vitro and in vivo experiments little or no attention has been paid to important issues like durability, clogging of the device and cleaning procedures of the vpe. During in vivo experiments Van der Torn et al. observed that the lip sometimes sticks to the interior of the cylindrical housing [37], but besides these observations no research has been done concerning these subjects, therefore no further conclusions can be drawn [8, 33].

As mentioned above, in vitro and in vivo experiments show us that we need to improve the behavior of the vpe, therefore numerical experiments might be very useful. The results of the numerical methods will be used to find the optimal geometry of the vpe. To validate these results in vitro and in vivo experiments can be used. When numerical and experimental methods are combined, the results of the experiments can help to guide and improve the numerical model, while in the numerical model several improvements can be investigated, without the trial and error approach using all sorts of prototypes [8].

Chapter 2

Development of the computational model

The computational models of the voice-producing element considered, consist of a single lip in a rectangular housing and an airflow along the top of this lip (figure 1.4). This field of science, involving problems with interactions between fluid (the airflow) and structure (the silicone rubber lip), is called fluid-structure interaction. In fluid-structure interaction fluid mechanics are coupled to structural mechanics (figure 2.1). Such a problem is called a coupled problem. More information about coupled problems can be found in appendix A.

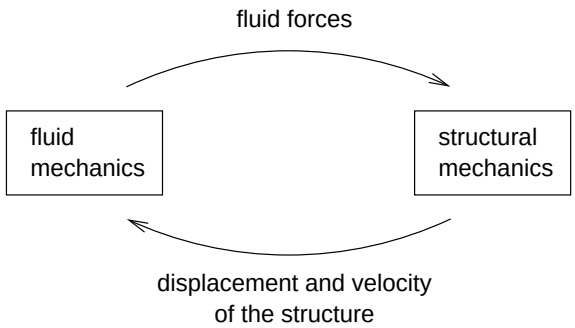

Figure 2.1: Interaction between fluid mechanics and structural mechanics

2.1 Two-dimensional computational model

At the moment there exist two working two-dimensional (2D) computational models of the vpe. The first working computational model was introduced by Hamburg and De Vries [16]. To realize the initial position of the lip Hamburg and De Vries used initial loads, which consisted of a force F_y and a moment M_z acting on the free end of the lip (figure 2.2).

De Vries tried to improve this computational model, by using a different damping of the silicone rubber lip, resulting in a different damping matrix C^{sys} in the mathematical equations (3.5). Furthermore, he tried to improve the model by using a different initial situation. Instead of initial loads acting on the free end of the lip, he used initial loads which are divided over the nodes (section 3.2.1) of the lip (figure 2.3).

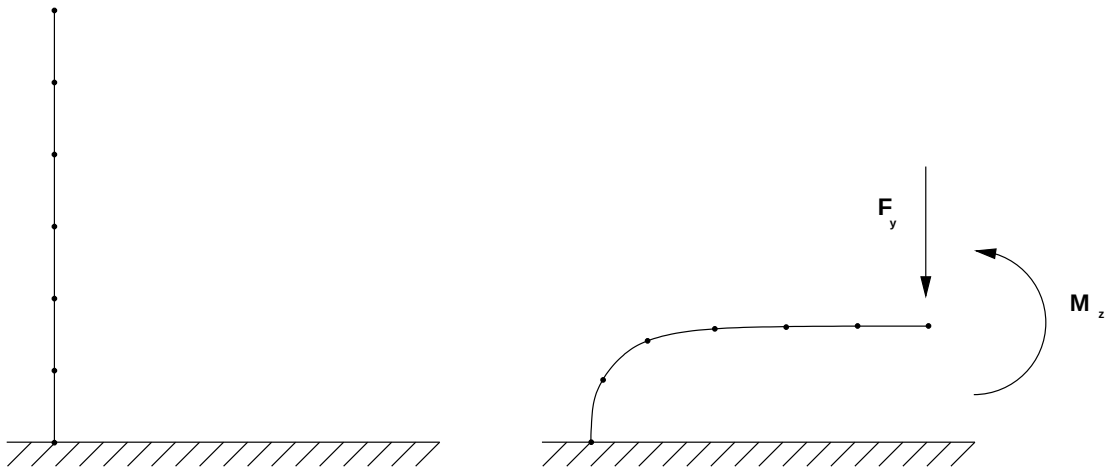

Figure 2.2: Lip in upright position and bent lip with initial loads on the free end of the lip

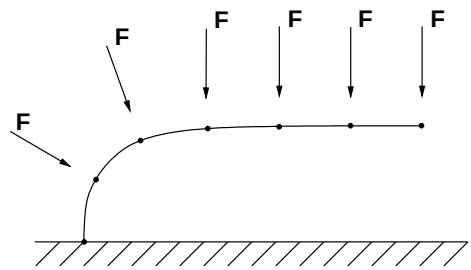

Figure 2.3: Bent lip with initial loads uniformly divided over the entire length of the lip

Unfortunately, there are many disadvantages of the 2D computational model of Hamburg and De Vries [8, 34]:

- In reality air flows along the sides of the lip. In the 2D model no simulation of this leakage along the lip is possible, because this model of the vpe contains no width.
- If the lip in the 2D model collides with the lower wall, air is enclosed. This results in the origination of extra forces. In reality these extra forces are limited, because air can flow along the sides of the lip to escape.
- To prevent breakdown of the computational model a precaution is taken, so that there is no collision possible with the lower wall, the wall in which the lip is inserted.
- During vibrations the silicone rubber lip can get twisted, which influences the sounds produced. Since the numerical model has only two dimensions, no torsion is allowed.

The second working 2D computational model is developed by Górska [14]. First, she improved the model of Hamburg and De Vries by inserting a pipe in the lower wall to prevent enclosure of air (figure 2.4). This way a solution had been found to realize collision of the silicone rubber lip with the lower wall in a 2D computational model, without breakdown of the model. Secondly, she inserted another pipe in the lower wall to simulate the airflow along the sides of the lip (figure 2.5).

Figure 2.4: A pipe (pipe2) applied in the model of Górska to prevent the enclosure of air

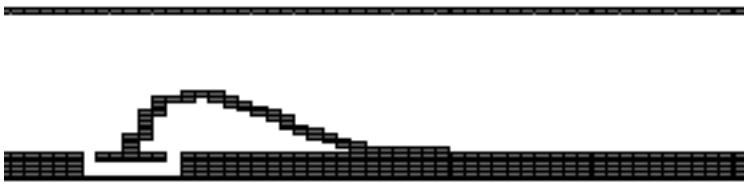

Figure 2.5: A pipe (pipe1) applied in the model of Górska to model leakage along the lip

The introduction of the pipes in the lower wall solved most of the flaws of the 2D model of Hamburg. The next step is to develop a three-dimensional (3D) computational model. In the 3D model width is added to allow airflow along the sides of the lip, so that examination of the influence of this airflow is possible.

2.1.1 The vocal tract, the subglottal tract and the shunt valve

Both existing 2D computational models only model the vpe. They both lack the representation of a vocal tract, a subglottal tract and a shunt valve.

The vocal tract consists of those areas of the vocal system above the larynx, comprising the pharynx, the oral cavity and the nasal cavity [8]. Unfortunately only little information could be found concerning the consequences of the neglect of the vocal tract in the computational models. The principal function of the vocal tract is transforming voice in voiced speech. During these transformations the vocal tract is a resonator, i.e. instead of a decrease of the sound pressure level due to the longer distance the sound has to travel, the overall SPL will increase because of the amplification of specific frequencies [30]. Both existing computational models neglect an acoustic resonator function and the SPL is calculated by the flow on the end of the housing of the vpe alone.

In vitro experiments showed that the influence of the subglottal tract, i.e. the trachea and the lungs, on the functioning of the vpe is negligible. It has no significant effect on any of the relations between flow, pressure, frequency and sound pressure level [8, 34].

Placing the vpe in a shunt valve lowers the $F0$ and results in a higher airflow resistance [8, 34].

Because we are still at the beginning of the development of a good computational model of a vpe, we will not include a representation of a vocal tract, a subglottal tract or a shunt valve. In future these representations might be included in the computational model. Although, we must be aware that when the results of the computational models are validated by experimental methods, the results of both models may differ from the results of in vitro and in vivo experiments [8, 33, 34], if the experiments involve a vocal tract, a subglottal tract or a shunt valve.

2.2 Three-dimensional computational model

When developing a computational model, such as our 3D computational model, there are several aspects to deal with [6]:

- numerical stability of the model;
- accuracy of the calculations;
- growing complexity of the problems;
- limited computing time and computer memory;
- limited development time, so try to make use of existing code.

To develop our 3D computational model, we will make use of two existing models. For the structural part we will use the 2D computational model of Górska, but instead of the pipes in the bottom of the housing to simulate the flow along the sides of the lip, we will add a third dimension, namely the width. For the fluid part we will use the 3D simulation method Comflo [13].

We will use a different initial situation then used by Górska and De Vries. Like De Vries we will use initial loads which are divided over the nodes of the lip, but instead of forces we will use moments (figure 2.6). When a beam is bent moments originate that are proportional to the local deflection of the beam. Therefore, we choose an initial load existing of moments.

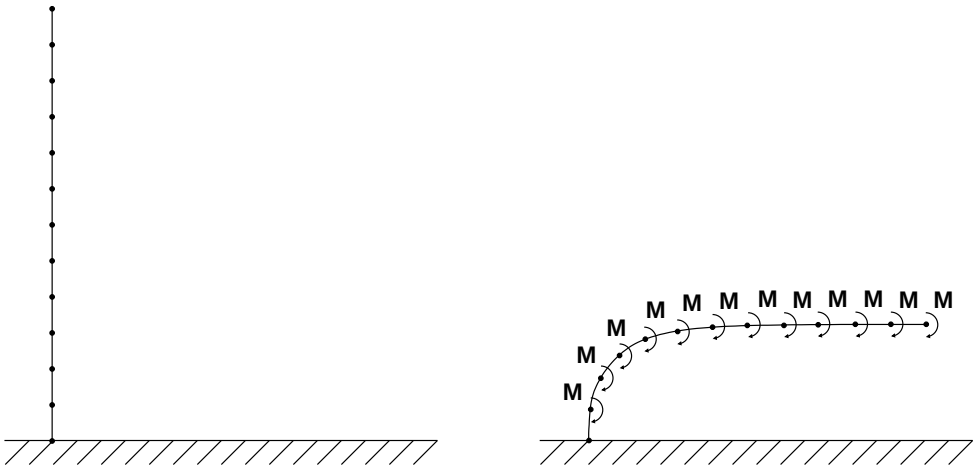

Figure 2.6: Lip in upright position and bent lip with initial moments uniformly divided over the entire length of the lip

This way every node of the beam knows directly how much it is bent and how much it likes to stretch [36].

The disadvantage of our 3D computational model is that there is still no torsion of the silicone rubber lip allowed. As can be read in the next chapter, the silicone rubber lip is described by 2D equations (3.5). By adding a constant width to the lip, we obtain a 3D lip. Due to the 2D equations, it will not be possible to calculate torsion of the lip. If we want to calculate torsion, we have to develop new 3D equations for the lip.

More information about the developed 3D computational model lip3D of the vpe can be found in the corresponding guide [17].

2.3 Numerical solution algorithm

Our 3D computational model of the voice-producing element will be solved numerically with a loose coupling algorithm (section A.2.4). A loose coupling algorithm indicates that only once per time step an interaction between the fluid part and the structure part occurs. A schematic representation of solving our problem can be found in figure 2.7.

We have chosen this algorithm since it is rather easy to program and practical to start solving a coupled problem with. Unfortunately, the algorithm has several disadvantages. For example, a loose coupling method does not make use of internal iterations, meaning that it does not wait for the fluid-structure interaction to converge. Therefore errors arise and loss of order of accuracy occurs. Consequently no big time steps are possible, so there is a limitation of the feasible time step.

If we would use a predictor-corrector algorithm (section A.2.4) instead of a loose coupling algorithm our results would be more accurate and we would need less computing time. But since we are still in the beginning of developing a good 3D computational model, it is more practical to start with the plain loose coupling algorithm and improve the model later with the more complicated predictor-corrector algorithm.

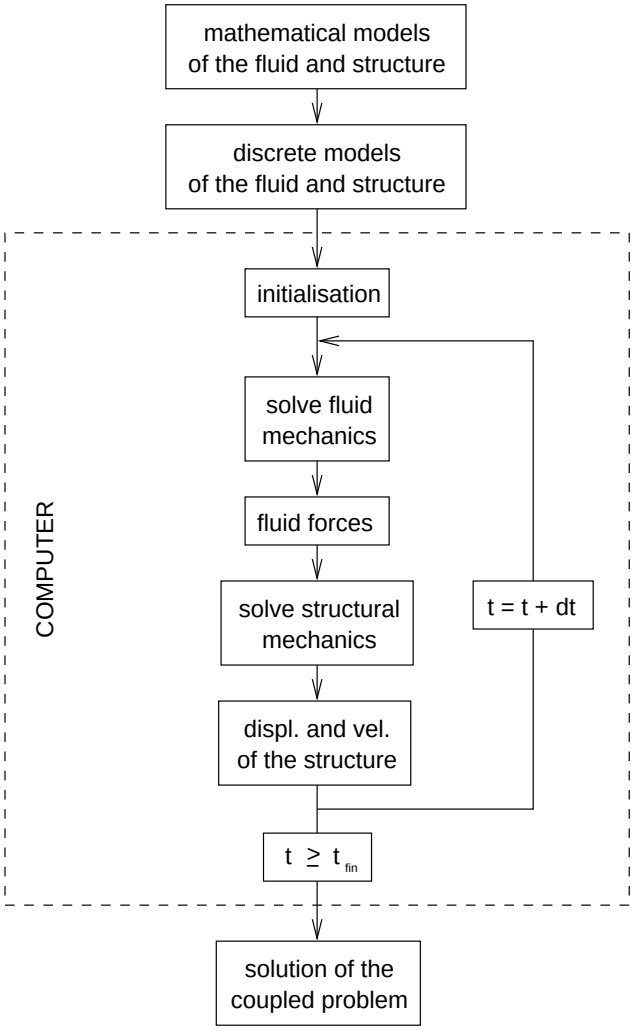

Figure 2.7: A schematic representation of solving the coupled problem of the vpe

Chapter 3

Detailed computational model

Our problem, a silicone rubber lip oscillating in an airflow, can also be called a three-field coupled problem [39], because it consists of three fields. Two physical fields represent the fluid and the structure, and one computational field represents the grid. The two physical fields are also discussed earlier (chapter 2).

3.1 The fluid

The fluid, i.e. the airflow, is described by the incompressible 3D Navier-Stokes equations, i.e. the conservation of mass and the conservation of moment [8, 14, 16], with the density ρ constant and p/ρ replaced by the pressure p.

- Conservation of mass (or continuity equation):

$$\text{div } \boldsymbol{u} = 0 \tag{3.1}$$

  with $\boldsymbol{u} = (u, v, w)$ the velocity vector.

- Conservation of moment:

$$\frac{\partial \boldsymbol{u}}{\partial t} + (\boldsymbol{u} \cdot \text{grad})\boldsymbol{u} = -\text{ grad } p + \nu \text{ div grad } \boldsymbol{u} + \boldsymbol{F} \tag{3.2}$$

  with p the pressure, ν the kinematic viscosity and $\boldsymbol{F} = (F_x, F_y, F_z)$ the vector representing the external forces on the fluid.

3.1.1 Computational grid

To solve the Navier-Stokes equations we first want to discretize (3.1) en (3.2). For the spatial discretization we will use a Cartesian grid, with the horizontal velocity u, the transverse velocity v and the vertical velocity w set in the middle of the cell faces (i.e. the boundary between two cells) and the pressure p set in the cell centres [8, 16]. This arrangement of the velocities and the pressure is called a staggered grid [35]. In figure 3.1 a 2D example is shown. Extension to a 3D staggered grid is straightforward.

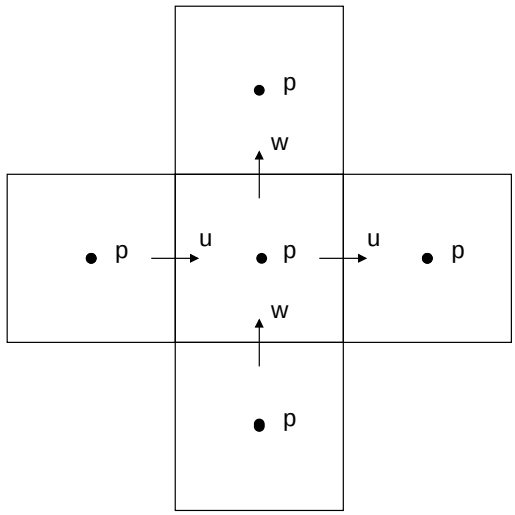

Figure 3.1: Location of the pressure and velocity components (2D)

3.1.2 Discretization in time

For the discretization in time (time integration method) the forward Euler method will be used. This results in rewriting the Navier-Stokes equations in the Poisson equation [8, 16]:

$$\text{div grad } p^{(n+1)} = \text{div}(\frac{\boldsymbol{u}^{(n)}}{\delta t} + \boldsymbol{R}^{(n)}) \tag{3.3}$$

with $\boldsymbol{R}^{(n)} = -(\boldsymbol{u}^{(n)} \cdot \text{grad})\boldsymbol{u}^{(n)} + \nu \text{ div grad } \boldsymbol{u}^{(n)} + \boldsymbol{F}^{(n)}$ and $(n+1)$, (n) denoting the new and old time level respectively.

3.1.3 Discretization in space

To solve partial differential equations numerically, discretization methods are used [2, 13]. We will solve our Poisson equation by a finite volume method [25, 35]. Therefore, we will have to rewrite (3.3) in conservation form (integral form). In this thesis we will not pay attention to this, but refer to Gerrits [13].

Discretizing the Poisson equation (3.3) results in the following [4]:

$$\begin{aligned} C_C\ P^{(n+1)}(i,j,k) &+ C_{XL}\ P^{(n+1)}(i-1,j,k) + C_{XR}\ P^{(n+1)}(i+1,j,k) \\ &+ C_{YL}\ P^{(n+1)}(i,j-1,k) + C_{YR}\ P^{(n+1)}(i,j+1,k) \\ &+ C_{ZL}\ P^{(n+1)}(i,j,k-1) + C_{ZR}\ P^{(n+1)}(i,j,k+1) \quad = f_C^{(n)} \end{aligned}$$

with

$$f_C^{(n)} = \text{div}(\frac{\boldsymbol{u}^{(n)}}{\delta t} + \boldsymbol{R}^{(n)}) \tag{3.4}$$

P is the approximation for the pressure and C_C, C_{XL}, ... represent the coefficients of the difference molecule [4]. A 2D example of the difference molecule is shown in figure 3.2. Extension to a 3D difference molecule is straightforward.

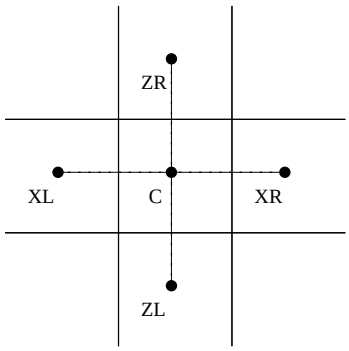

Figure 3.2: The points which belong to the coefficients of the difference molecule (2D)

For the discretization of the convective term

$$(\boldsymbol{u} \cdot \text{grad})\boldsymbol{u}$$

and the diffusive term

$$\nu \text{ div grad } \boldsymbol{u}$$

of $\boldsymbol{R}$ in (3.4) we will use upwind discretization and central discretization respectively [4, 35]. For more information about these discretizations we refer to Gerrits [13].

3.1.4 Solution method

To solve the discretized equation (3.1.3) numerically we will use an iterative solution method, namely the conjugate gradient (CG) method. To accelerate the solution process we will make use of preconditioning by using a Modified Incomplete LU (MILU) factorization. More information about these solution methods can be found in [4, 32].

3.2 The structure

In our numerical model the structure, i.e. the silicone rubber lip, is described by the following elastic equation [8, 14, 16]:

$$[M^{sys}] \cdot \ddot{\boldsymbol{V}}^{sys} + [C^{sys}] \cdot \dot{\boldsymbol{V}}^{sys} + [K^{sys}] \cdot \boldsymbol{V}^{sys} = Q^{q,sys} + Q^{\sigma,sys} \tag{3.5}$$

with $[M^{sys}]$ the mass matrix, $[C^{sys}]$ the damping matrix and $[K^{sys}]$ the stiffness matrix. $\boldsymbol{V}$ is the vector containing the displacements and rotations of the nodes of the lip. We will pay more attention to this vector in section 3.2.1. Finally $Q^{q,sys}$ and $Q^{\sigma,sys}$ are the vectors containing the nodal forces due to the air pressure and initial loads respectively.

As mentioned before (section 2.2), these elastic equation are 2D. By adding a third dimension, namely a constant width, we obtain a 3D lip.

3.2.1 Discretization in space

To solve the elastic equation we first want to discretize (3.5) by a finite element method [5]. I.e. the structure has to be divided in several elements. To describe the silicone rubber lip of

the vpe, several 2D-beam elements are used, connected to each other in nodes (figure 3.3). Instead of six elements in the past [16], we will use twelve elements to make sure the lip is slender and to obtain more realistic results, while the amount of computing time is still acceptable.

Each element has three degrees of freedom at each node concerning the movement of an element: the horizontal displacement u in the x-direction [1], the vertical displacement v in the z-direction and the rotation ϕ [8, 14, 16].

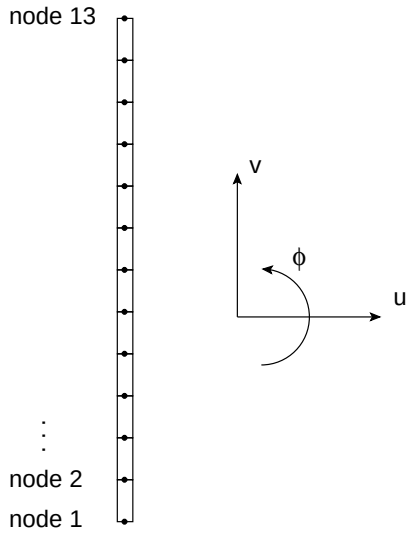

Figure 3.3: Lip in upright position consisting of 12 beam elements

In figure 3.4 the position of the lip, which is calculated by the ANSYS package and simulated by our computational model, is depicted.

In the elastic equation (3.5) the vector $\boldsymbol{V}$ will look like:

$$\boldsymbol{V} = \begin{Bmatrix} u_1 \\ v_1 \\ \phi_1 \\ \vdots \\ u_{13} \\ v_{13} \\ \phi_{13} \end{Bmatrix}$$

with u_i, v_i and ϕ_i denoting respectively the horizontal displacement, the vertical displacement and the rotation at node i.

3.2.2 Solution method

To solve the elastic equation numerically, we will use the Newmark-β method, a direct solution method. More information about this method can be found in [16].

[1] The displacements u and v should not be confused with the velocity $\boldsymbol{u} = (u, v)$ in the Navier-Stokes equations (3.1) and (3.2).

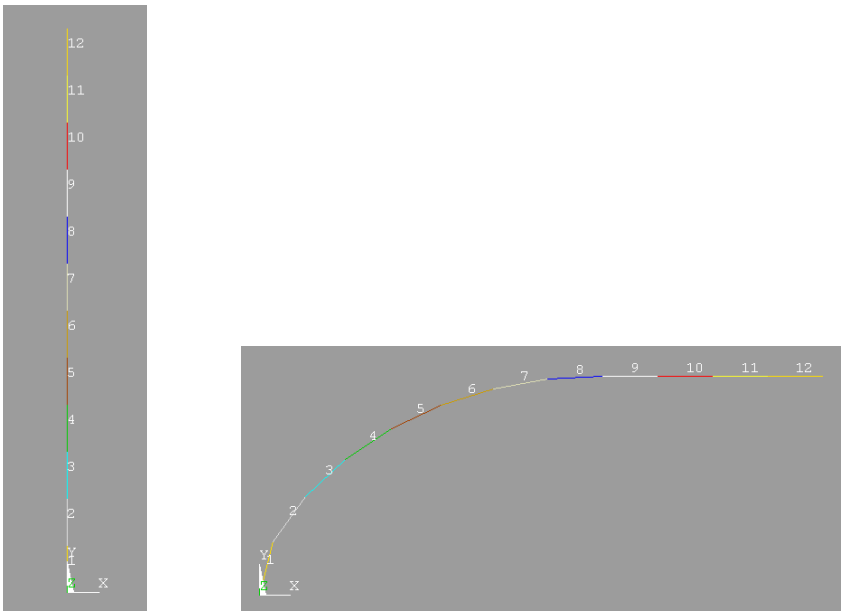

Figure 3.4: Lip in upright position and bent lip calculated by ANSYS

3.3 The grid

Most about the grid has already been mentioned in subsection 3.1.1. To make distinction between the structure, the fluid and the boundary, the cells are labeled. In this report we will pay no attention to the way this labeling occurs, since it is rather complex. For more information we refer to Gerrits [13] or Fekken [11]. This labeling has to be updated every time step.

3.4 The flow of information

Now that we have explained the three fields of our coupled problem of the vpe, we can tell more about the exchange of data between the fluid, the structure and the grid in our numerical model. A schematic overview can be seen in figure 3.5. This exchange of data occurs in the same way as with a block Gauss-Seidel scheme (A.2.3), i.e. the fields are solved alternately and in between the data is exchanged. For example, the fluid forces have to be passed on to the structure, so that the new position and velocity of the structure can be computed. According to this new position and velocity of the structure, the labeling of the grid can be updated and the fluid forces at the next time step can be computed [39].

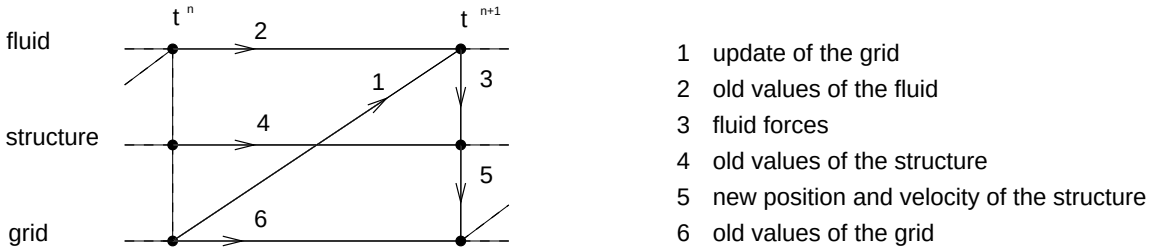

Figure 3.5: The flow of information between fluid, structure and grid

3.5 Data

An overview of variables used in our computational model, which correspond to the values used in the in vitro experiments (chapter 6):

length lip	8.61 mm
width lip	4.75 mm
height lip	0.266 mm
elasticity lip	between $1.3 \cdot 10^6$ and $4.0 \cdot 10^6$ Pa
density lip	$1.13 \cdot 10^3 \ \frac{kg}{m^3}$
number of elements	12
origin clamping	8.167 mm
length housing	4.738 cm
width housing	4.93 mm
height housing	3.01 mm
ν_{air}	$1.33 \cdot 10^{-5} \ \frac{m^2}{s^2}$
ρ_{air}	$1.2 \ \frac{kg}{m^3}$

Chapter 4

Verification

To verify the numerical stability of the 3D computational model lip3D, the influences of different numerical quantities will be investigated. These influences will affect the numerically accuracy of the computational model. Examples are different compilers (section 4.1), different values for epsilon ϵ (section 4.2), different time steps by influencing the Courant-Friedrichs-Levy number (section 4.3) and different grids (section 4.4).

A standard simulation is needed to investigate the influences of these different quantities on the results of the model. This way the results can be compared with another. Notice that only one influence can be examined at a time, i.e. the corresponding value in the computational model may vary, while all other values have to maintain constant. The standard simulation has a run time of 36 minutes if it is performed on a Celeron@1GHz. This simulation has the following values.

ϵ	$1.0 \cdot 10^{-7}$
CFL-max	0.5
CFL-min	0.2
grid	96 x 1 x 30 cells (2D); 0.95 stretch in z-direction
dimension	2D
c_{mass}	$89.5\ \frac{1}{s}$
c_{stiff}	$8.0 \cdot 10^{-4}\ s$
E	$6.0 \cdot 10^{6}\ Pa$
P	$500\ Pa$

More information about these quantities can be found in the following sections and in chapter 5.

The flow Q, the fundamental frequency $F0$ and the sound pressure level SPL will be calculated to compare the results of the different simulations. The computation of these quantities is described by Górska [14]. The flow plots of the different simulations belonging to the same quantity investigation will be plotted in one picture. The legend of the picture will show the number of flow plots depicted, since it might be possible that some plots will coincide.

The calculated flow of our standard simulation can be seen in figure 4.1. This graph corresponds to the amount of fluid per second ($\frac{m^3}{s}$) that passes the end of the vpe. Clearly, this amount of fluid depends on the oscillations of the lip. If the lip is pressed to the top of the

housing, no fluid is able to pass the lip (the standard simulation is 2D, so there are no slits along the sides of the lip). Consequently, the flow will be zero. If the lip reaches its lowest position in the housing, the flow will become maximal.

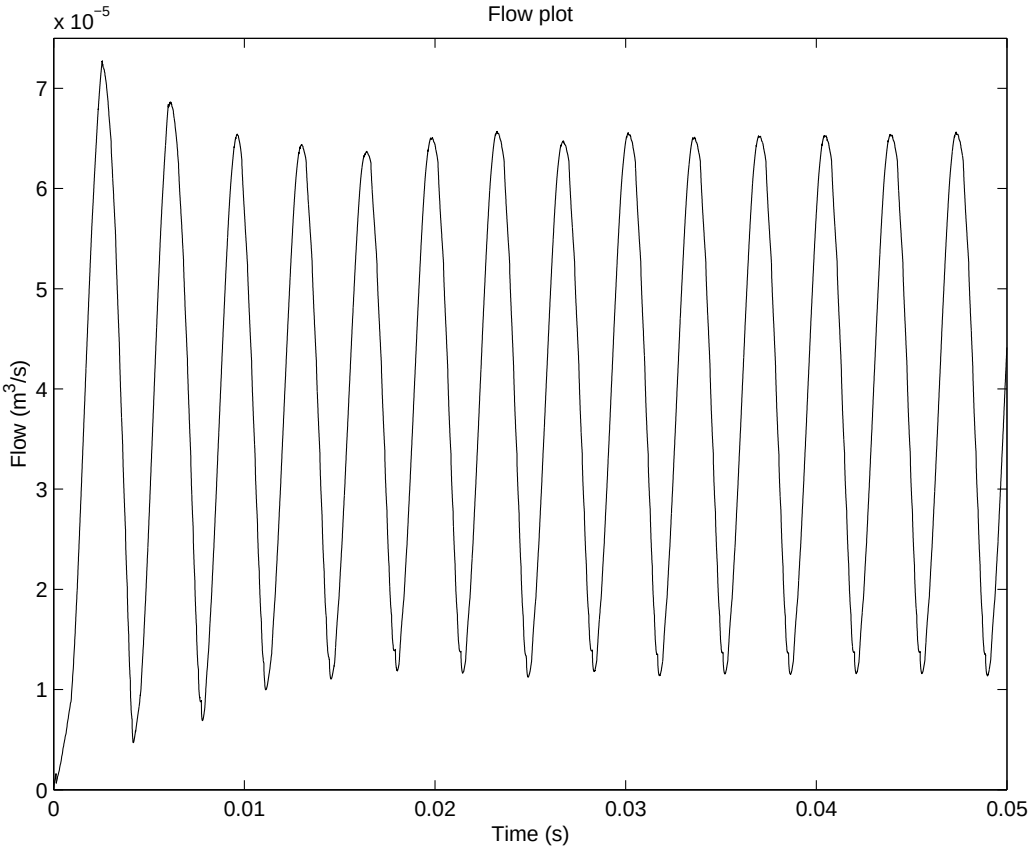

Figure 4.1: Flow plot comprising the standard simulation

In the standard simulation the lip needs five oscillations to become stable, as can be seen in figure 4.1. For the calculation of the $F0$ and the SPL only the stable oscillations will be used.

Standard simulation

$F0 = 290\ Hz$	$SPL = 59\ dB$

In the following sections the flow, the $F0$ and the SPL will be calculated for different simulations. To compare the results of these different simulations all flow plots will be plotted in the same figure and percentages will indicate the deviation of the calculated $F0$ and SPL from the $F0$ and SPL of the standard simulation. To loose as little information as possible these percentages will be calculated by using $F0$ and SPL values in four decimals to result in a percentage in one decimal.

4.1 Compiler

A compiler is required to make a computational model executable. Compiler options can be used, for example, to influence the level of optimization, vectorization or parallelization.

Normally compiler options have little or no influence on the results of a computational model. However, when different compiler options for the compiler f77 are used, the results of the computational model lip3D appear to differ. To verify the obtained results, the model was tested in the Centre for High Performance Computing & Visualization (HPC&V) on the vector supercomputer Cray SV1e with the compiler f90 [1].

The flow plots, which belong to the results of the compilers f77 and f90, can be found in figure 4.2. The compiler options -O and -O2 for the compiler f77 are used to increase the optimization level of the compilation, whereas -Ovector3 for the compiler f90 is used to increase the vectorization of the code.

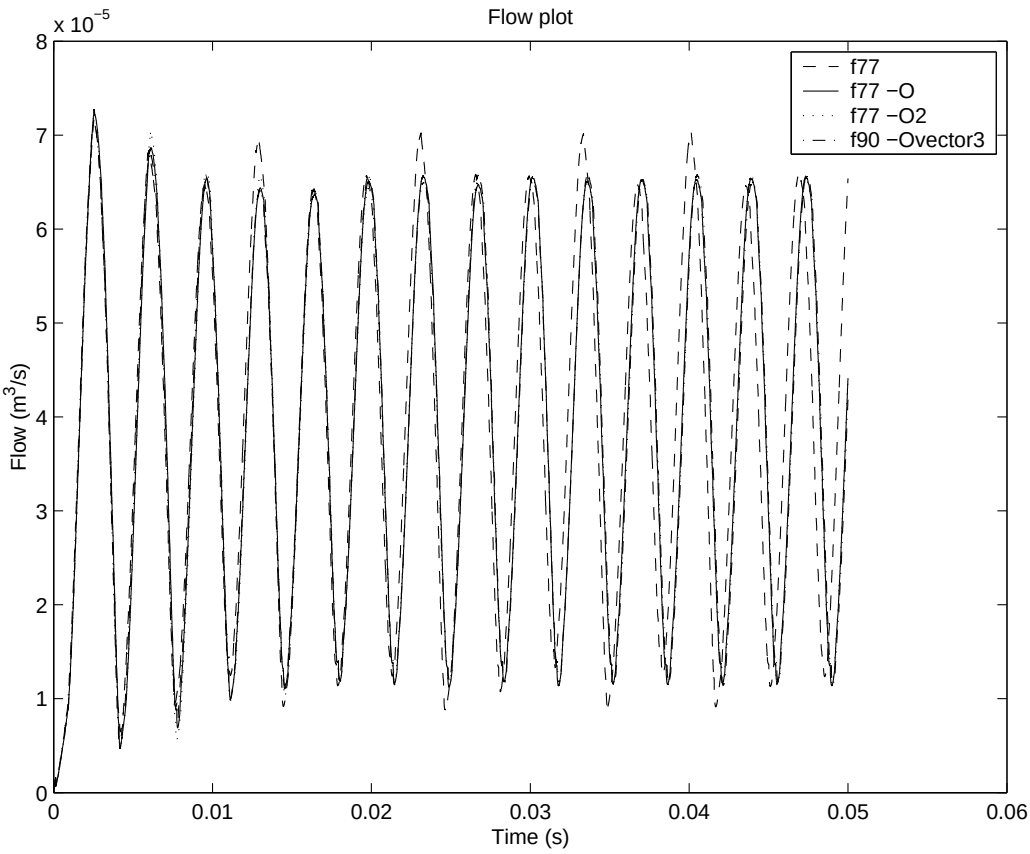

Figure 4.2: Flow plot comprising different compilers

The values of the $F0$ and SPL which belong to the compilers f77, f90 and their compiler options are mentioned below.

Compiler: f77

$F0 = 294\ Hz$	$SPL = 59\ dB$

Compiler: f77 -O (standard simulation)

$F0 = 290\ Hz$	$SPL = 59\ dB$

Compiler: f77 -O2

$F0 = 290\ Hz$	$SPL = 59\ dB$

Compiler: f90 -Ovector3

$F0 = 290\ Hz$	$SPL = 59\ dB$

The flow plots and calculated values of the $F0$ and the SPL show that using optimization during the compilation affects the flow and the $F0$. Moreover, it can be seen that the results of f77 -O most closely resemble the results acquired by the Cray. Since two completely different compilers give approximately the same results, the compiler f77 with the compiler option -O will be used for further compilation of the computational model lip3D. An attractive side effect is the decrease of the computation time with almost a factor seven if optimization is used during the compilation.

4.2 Epsilon

In section 3.1 is described how the Poisson equation (3.3) in the computational model lip3D is solved by using the CG method and MILU factorization. The quantity epsilon ϵ is used to determine the accuracy with which the Poisson equation will be solved. The smaller the value for ϵ, the more iterations will be used to solve the Poisson equation and the more numerically accurate the results will become. More precise, ϵ is the iteration error that is allowed to solve the Poisson equation.

If different values for ϵ have no or only little influence on the standard simulation, the computation of the pressure in the standard simulation is accurate. The flow plots of these different simulations can be found in figure 4.3.

The values of the $F0$ and the SPL belonging to the different simulations are presented below.

$\epsilon = 1.0 \cdot 10^{-6}$

$F0 = 291\ Hz$ [0.1 %]	$SPL = 59\ dB$ [0.0 %]

$\epsilon = 1.0 \cdot 10^{-7}$ (standard simulation)

$F0 = 290\ Hz$	$SPL = 59\ dB$

$\epsilon = 1.0 \cdot 10^{-8}$

$F0 = 290\ Hz$ [0.0 %]	$SPL = 59\ dB$ [0.0 %]

As can be seen in the flow plots and by the values of $F0$ and SPL, the different values for ϵ have no significant influence on the standard simulation. Therefore, the Poisson equation (3.3) is solved precisely, i.e. that the computation of the pressure is accurate.

4.3 Courant-Friedrichs-Levy number

During its computations the model lip3D uses adaptive time steps [11, 16]. If the fluid or structure is moving very wildly, time steps have to be smaller than when the fluid is moving calmly. It is useful to adjust the time steps to these changes to achieve a more numerically accurate computation (smaller time steps) and an improvement of the computation time (bigger time steps). Therefore, the Courant-Friedrichs-Levy (CFL) number is introduced.

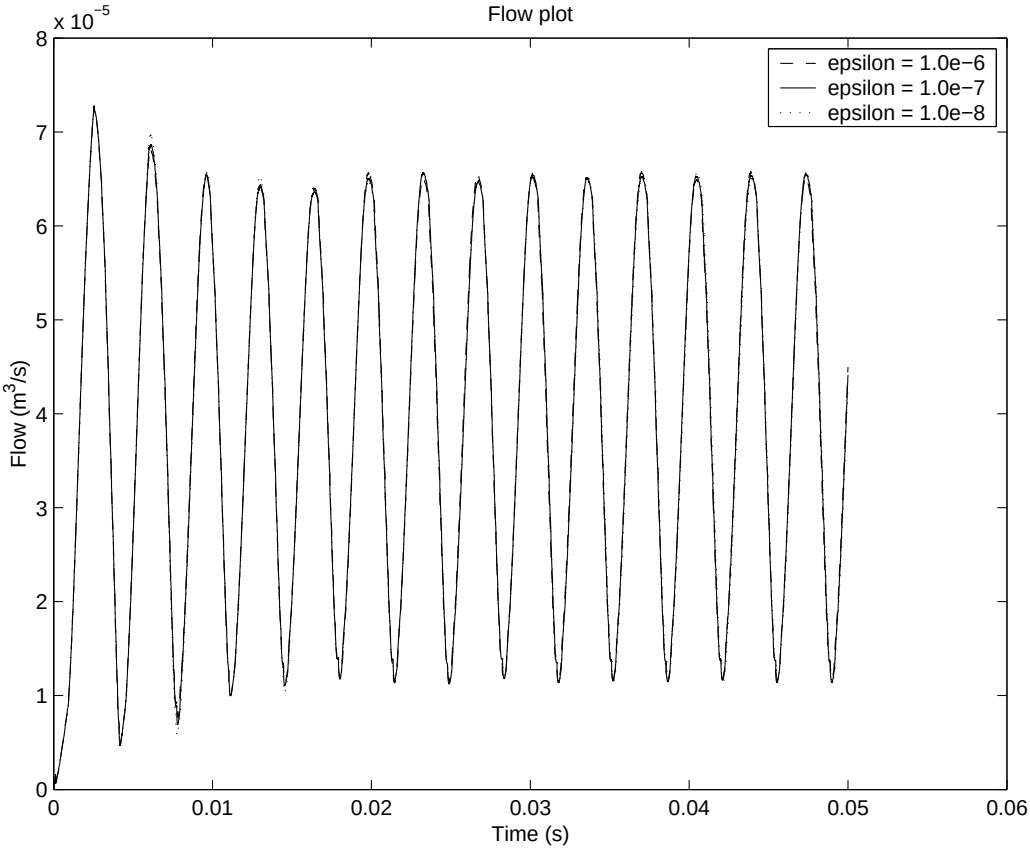

Figure 4.3: Flow plot comprising different values for epsilon

$$CFL = \frac{|u|\delta t}{h_x} + \frac{|v|\delta t}{h_y} + \frac{|w|\delta t}{h_z}$$

with $\boldsymbol{u} = (u, v, w)$ the velocity, h_x, h_y and h_z the distances between the cell centers in x-, y- and z-direction respectively and δt the time step.

If the movement of the fluid or structure becomes wilder (high values for $|u|$, $|v|$ or $|w|$) or if the computation is done on a very fine grid (small values for h_x, h_y or h_z), the CFL-number increases. If the CFL-number increases above a prescribed value CFL-max, the time step will be halved. If the CFL-number decreases under a prescribed value CFL-min, the time step will be doubled. At the end of every time step the model calculates this CFL-number and determines whether the time step is correct, needs to be halved or can be doubled.

The integration of time in the standard simulation is accurate if different values for CFL-max and CFL-min have a negligible influence on the results of the standard simulation. In figure 4.4 the flow plots of different values for CFL-max and CFL-min are depicted.

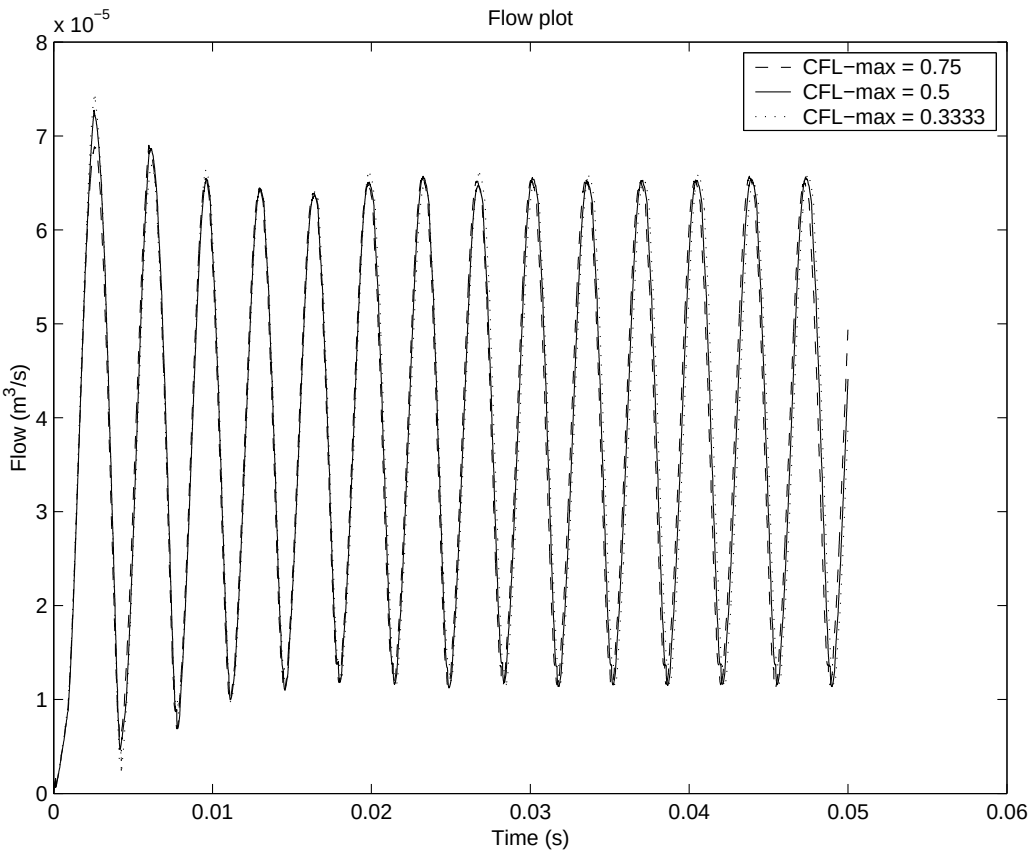

Figure 4.4: Flow plot comprising different values for the CFL number

The various simulations concerning CFL-max and CFL-min have the following values for the $F0$ and the SPL.

CFL-max = 0.75, CFL-min = 0.3

$F0 = 291\ Hz$ [0.4 %]	$SPL = 59\ dB$ [0.5 %]

CFL-max = 0.5, CFL-min = 0.2 (standard simulation)

$F0 = 290\ Hz$	$SPL = 59\ dB$

CFL-max = 0.3333, CFL-min = 0.1333

$F0 = 290\ Hz$ [0.1 %]	$SPL = 59\ dB$ [0.2 %]

The obtained results indicate that different values of CFL-max and CFL-min have a negligible influence on the results of the standard simulation. Therefore it can be concluded that the time integration in the standard simulation is accurate.

4.4 Grid research

Because the numerically accuracy and computation time of a simulation depend largely on the grid, a lot of attention has been paid to grid research. In general, a finer grid will result in more numerically accurate results, while a coarser grid will result in a smaller computation time. Consequently, a rather fine grid is preferred, so that the results are numerically accurate, but with still as less computation time as possible. The results of a simulation are called numerically accurate if grid refinement has no significant influence on the results.

First, attention will be paid to coarse grids. In figure 4.5 the standard simulation and simulations with grids consisting of less than 96 by 1 by 30 cells are depicted. The corresponding values for the $F0$ and SPL can be found below.

grid = 96 x 1 x 30 cells (2D); 0.95 stretch in z-direction (standard simulation)

$F0 = 290\ Hz$	$SPL = 59\ dB$

grid = 72 x 1 x 23 cells (2D); 0.9333 stretch in z-direction

$F0 = 268\ Hz$ [7.6 %]	$SPL = 62\ dB$ [5.0 %]

grid = 64 x 1 x 20 cells (2D); 0.925 stretch in z-direction

$F0 = 238\ Hz$ [18.0 %]	$SPL = 63\ dB$ [6.3 %]

grid = 48 x 1 x 15 cells (2D); 0.9 stretch in z-direction

$F0 = 222\ Hz$ [23.7 %]	$SPL = 63\ dB$ [6.8 %]

The results differ significantly. The coarse grids result in dissimilar amounts of fluid per second (figure 4.5), $F0$ values which differ more than 5 procent from the standard simulation and SPL values which differ 3 dB or more. Therefore, it can be concluded that the results of the grids consisting of 72 by 1 by 23 cells, 64 by 1 by 20 cells and 48 by 1 by 15 cells are numerically inaccurate.

Second, attention will be paid to grid refinement. In figure 4.6 the standard simulation and simulations with grids consisting of more than 96 by 1 by 30 cells are depicted. The corresponding values for the $F0$ and SPL can be found below.

grid = 144 x 1 x 45 cells (2D); 0.9667 stretch in z-direction

$F0 = 293\ Hz$ [1.0 %]	$SPL = 61\ dB$ [3.5 %]

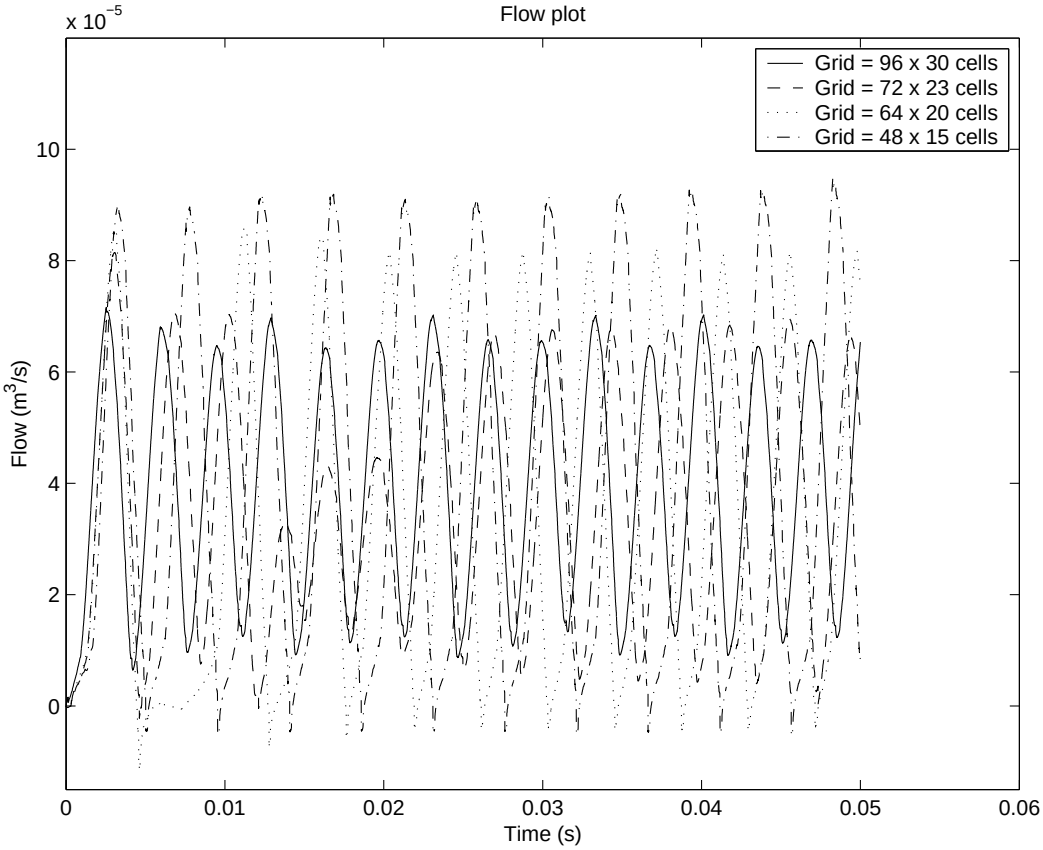

Figure 4.5: Flow plot comprising the standard grid and different coarse grids

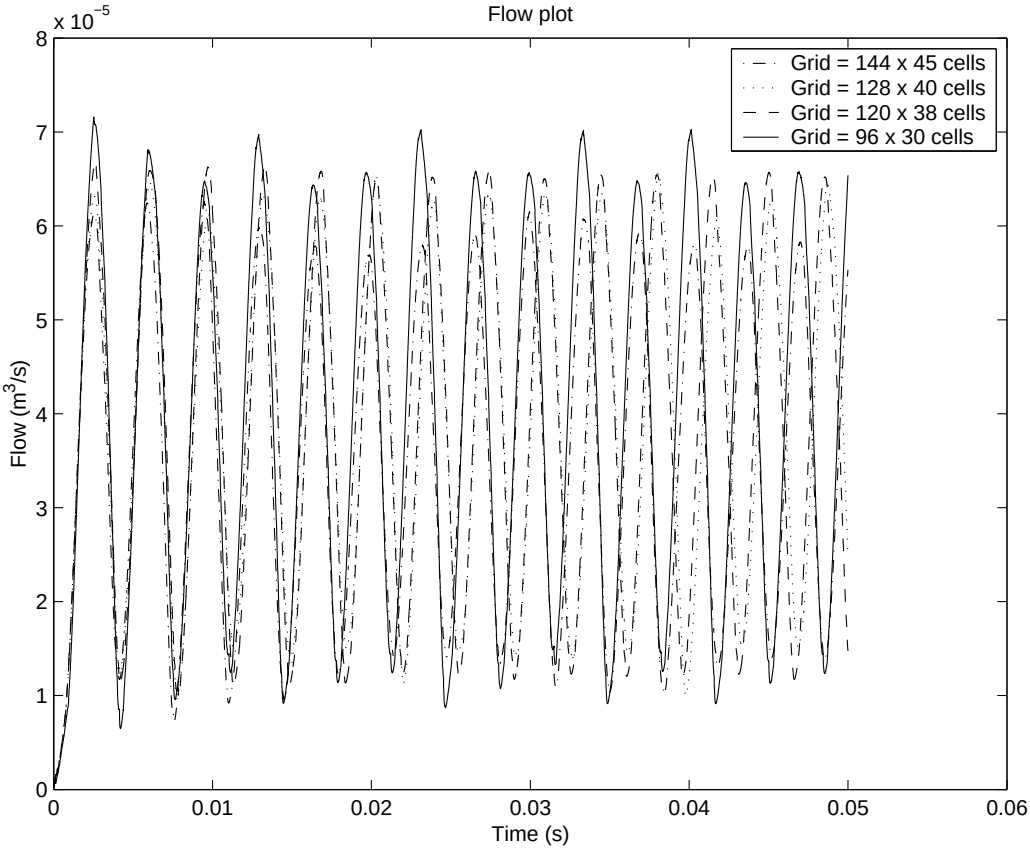

Figure 4.6: Flow plot comprising the standard grid and different fine grids

grid = 128 x 1 x 40 cells (2D); 0.9625 stretch in z-direction

$F0 = 281\ Hz$ [3.2 %]	$SPL = 60\ dB$ [1.9 %]

grid = 120 x 1 x 38 cells (2D); 0.96 stretch in z-direction

$F0 = 283\ Hz$ [2.5 %]	$SPL = 60\ dB$ [2.3 %]

grid = 96 x 1 x 30 cells (2D); 0.95 stretch in z-direction (standard simulation)

$F0 = 290\ Hz$	$SPL = 59\ dB$

The flow plots, $F0$ values and SPL values indicate that grid refinement has an insignificant influence on the results of the standard simulation. I.e. the flow plots correspond to each other, the $F0$ values differ less than 5 percent and the SPL values differ less than 3 dB. Consequently, the results obtained by a grid consisting of 96 by 1 by 30 cells are numerically accurate.

If more grid refinement is applied, different results are acquired. In figure 4.7 the flow plots of these simulations are depicted. Below the figure the corresponding $F0$ values and SPL values are mentioned.

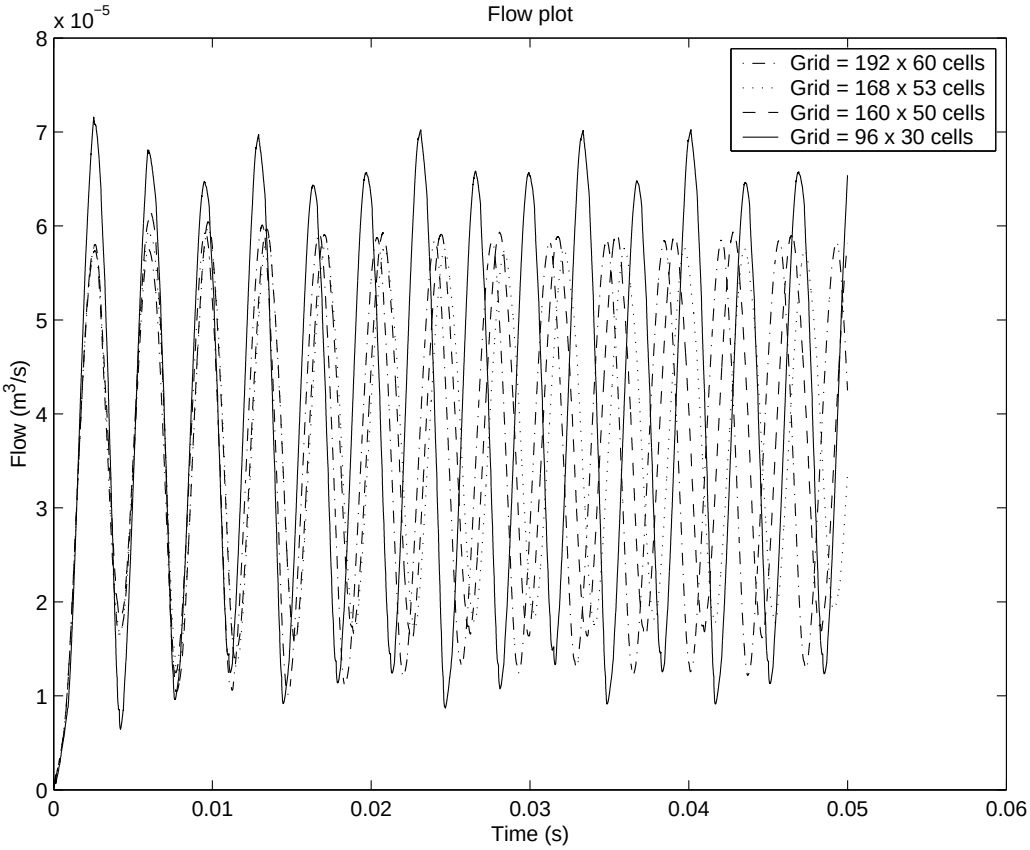

Figure 4.7: Flow plot comprising the standard grid and different finer grids

grid = 192 x 1 x 60 cells (2D); 0.975 stretch in z-direction

$F0 = 275\ Hz$ [5.2 %]	$SPL = 60\ dB$ [1.7 %]

grid = 168 x 1 x 53 cells (2D); 0.9714 stretch in z-direction

$F0 = 264\ Hz$ [9.0 %]	$SPL = 59\ dB$ [0.9 %]

grid = 160 x 1 x 50 cells (2D); 0.97 stretch in z-direction

$F0 = 271\ Hz$ [6.7 %]	$SPL = 60\ dB$ [1.4 %]

grid = 96 x 1 x 30 cells (2D); 0.95 stretch in z-direction (standard simulation)

$F0 = 290\ Hz$	$SPL = 59\ dB$

The results, especially the $F0$ values which differ more than 5 percent, show that strong grid refinement has too much influence on the results of the standard simulation to be neglected. Normally, more grid refinement would produce more numerically accurate results. However, in our case the lip is a restrictive factor because, in spite of grid refinement, the lip will always be represented by one cell. With strong grid refinement, this will influence the results more than with normal grid refinement. Therefore, it is questionable whether the obtained results are numerically accurate.

Since the results of coarse grids are numerically inaccurate and because it is questioned whether the results of strong grid refinement are numerically accurate, normal grid refinement shows that the grid consisting of 96 by 1 by 30 cells produces numerically accurate results with as less computation time as possible.

Of the investigated quantities of this chapter and the next, grid research has the biggest influence on the run time of the simulations. To give an impression of the influence of the number of grid cells on the run time of the simulations: a standard simulation, with a grid of 96 x 1 x 30 cells, has a run time of 36 minutes on a Celeron@1GHz, while a grid consisting of half the number of cells, i.e. 48 x 1 x 15 cells, has a run time of 4 minutes and a grid consisting of double the number of cells, i.e. 192 x 1 x 60 cells, has a run time of 9 houres and 52 minutes.

4.5 Conclusions

To verify the numerical stability of the 3D computational model lip3D, the influences of different numerical quantities are investigated. The investigation of the influence of ϵ shows that the computation of the pressure in the standard simulation is accurate. The investigation of different time steps by influencing the CFL-number indicates that the time integration in the standard simulation is accurate. Finally, based on gaining approximately the same results with different compilers and based on grid research it may be concluded that the results obtained by the standard simulation are numerically accurate.

Because the model lip3D is only little affected by small changes to ϵ, CFL-max, CFL-min and the grid, the model is called numerically stable. Moreover, the 2D results obtained by the computational model lip3D are similar to the results obtained by the 2D computational model lip of Górska, even though the models use different grids, different iterative solvers and different lengths of the housing. Consequently, the model lip3D is considered to be reliable.

Chapter 5

Parameter study

To examine the performance of the computational model lip3D, the influence of different parameters will be investigated. First, parameters will be investigated that will alter the properties of the silicone rubber lip. Examples are the damping coefficients c_{mass} and c_{stiff} (section 5.1) and the elasticity modulus E (section 5.2). Second, a parameter will be investigated that will affect the flow, namely the prescribed entrance pressure P (section 5.3). Finally, the influence of different numbers of dimensions will be investigated (section 5.4).

In section 5.4.1 it is investigated whether a 3D computational model is necessary or whether a 2D computational model is sufficient.

For the parameter study the same standard simulation will be used as mentioned in chapter 4. Notice again that only one parameter can be examined at a time, i.e. the corresponding value in the computational model may vary, while all other values have to maintain constant.

5.1 Damping coefficients

The damping matrix $[C^{sys}]$ of the elastic equation (3.5) is calculated by [14]

$$[C^{sys}] = c_{mass} \cdot [M^{sys}] + c_{stiff} \cdot [K^{sys}]$$

with c_{mass} and c_{stiff} the damping coefficients depending only on the material properties.

To determine the values for the damping coefficients c_{mass} and c_{stiff} of the silicone rubber, De Vries and Hamburg could find no useful information in the literature. As a result, they adjusted the values to match the results of their in vitro experiments.

In the following sections the results of different values for c_{mass} and c_{stiff} will be investigated. Since it is questioned whether the dampings coefficients should be scaled with the elasticity modulus (section 5.2), c_{mass} and c_{stiff} will be scaled by the factor $\frac{8.6 \cdot 10^6\ Pa}{6.0 \cdot 10^6\ Pa} = 1.4333$, i.e. the value used by Hamburg and De Vries divided by the current value.

5.1.1 c_{mass}

The damping coefficient c_{mass} is a parameter that damps the low frequencies of the silicone rubber lip. If c_{mass} increases, there will be more damping of the lip. For more information reference should be made to Clough and Penzien [7].

The flow plots corresponding to different values of c_{mass} can be found in figure 5.1. The values for the $F0$ an SPL belonging to these different simulations are mentioned below.

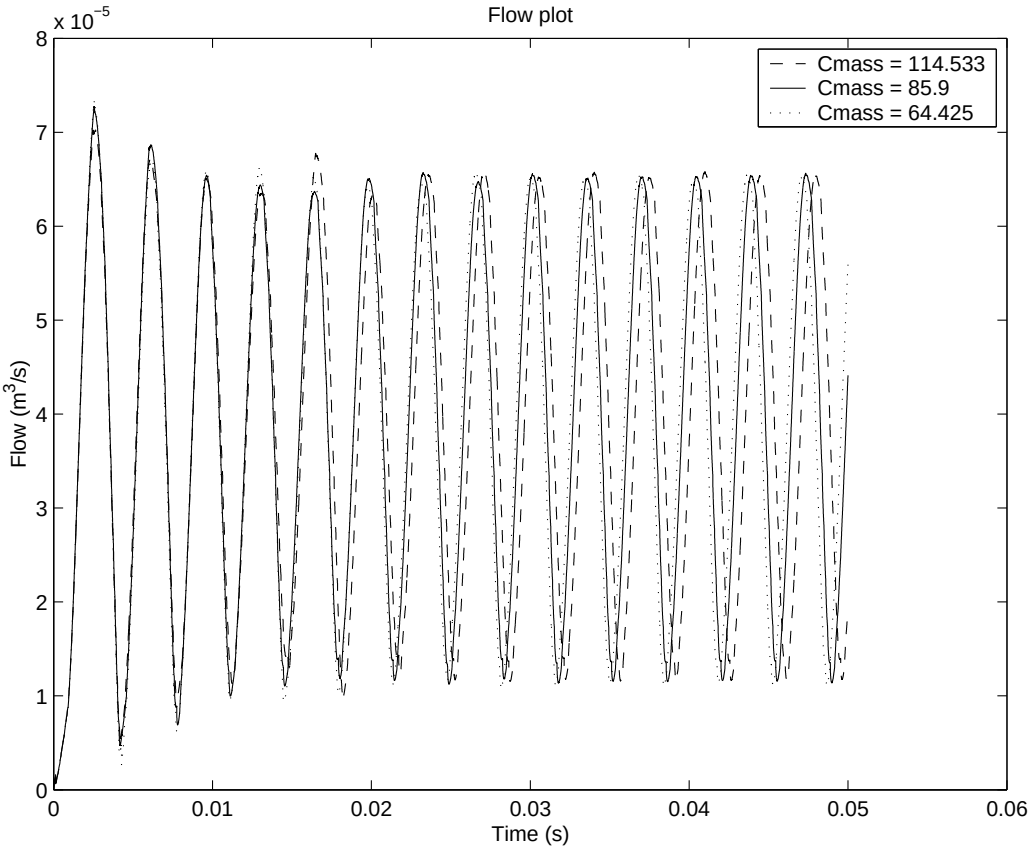

Figure 5.1: Flow plot comprising different values for c_{mass}

$c_{mass} = 114.533 \ \frac{1}{s}$

$F0 = 287 \ Hz$ [1.0 %]	$SPL = 59 \ dB$ [0.0 %]

$c_{mass} = 89.0 \ \frac{1}{s}$ (standard simulation)

$F0 = 290 \ Hz$	$SPL = 59 \ dB$

$c_{mass} = 64.425 \ \frac{1}{s}$

$F0 = 293 \ Hz$ [0.8 %]	$SPL = 59 \ dB$ [0.1 %]

From the flow plot, the $F0$ values and the SPL values it may be concluded that the influence of c_{mass} on the results of the standard simulation is negligible.

5.1.2 c_{stiff}

The damping coefficient c_{stiff} is a parameter that damps the high frequencies of the silicone rubber lip. An increase of c_{stiff} will result in more damping of the lip. For more information reference should be made to Clough and Penzien [7].

In figure 5.2 the flow plots of different values for c_{stiff} are depicted. The values for the $F0$ and the SPL of the various simulations can be found below.

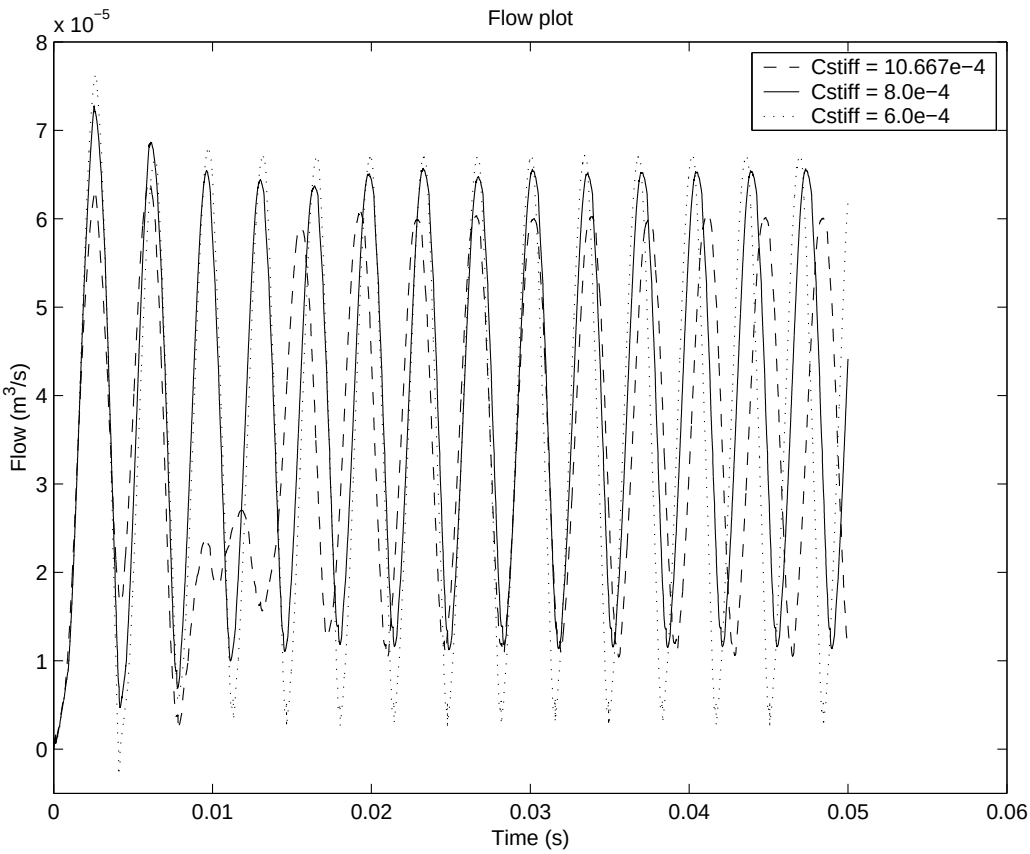

Figure 5.2: Flow plot comprising different values for c_{stiff}

$c_{stiff} = 10.667 \cdot 10^{-4}\ s$

$F0 = 274\ Hz$ [5.5 %]	$SPL = 61\ dB$ [3.0 %]

$c_{stiff} = 8.0 \cdot 10^{-4}\ s$ (standard simulation)

$F0 = 290\ Hz$	$SPL = 59\ dB$

$c_{stiff} = 6.0 \cdot 10^{-4}\ s$

$F0 = 296\ Hz$ [1.9 %]	$SPL = 61\ dB$ [3.0 %]

The results for different values for the damping coefficient c_{stiff} show that c_{stiff} has little influence on the results of the standard simulation. I.e. the flow plots differ only a little, the $F0$ values differ about 5 percent and the SPL values differ less than 3 dB.

Finally, since the damping coefficients c_{mass} and c_{stiff} are scaled by the same factor for this research, it can be concluded that c_{stiff} has more influence on the results of the standard simulation than c_{mass}. Consequently, more attention has to be paid to the damping coefficient c_{stiff} than to c_{mass}.

5.2 Elasticity modulus

The silicone rubber lip of the vpe has an elasticity modulus between $1.3 \cdot 10^6$ and $4.0 \cdot 10^6$ Pa according to the manufacturer. However, in the computational model lip3D a lip with an elasticity modulus of $6.0 \cdot 10^6$ Pa is used.

A flexible lip (small elasticity modulus) is able to move over a greater distance in the same amount of time than a stiff lip (high elasticity modulus). However, our model is very sensitive to large movements of the lip, i.e. movements that skip one or more cells. Therefore, lip3D uses large elasticity moduli to make sure that the movements of the lip are small and the model is stable.

To investigate the influence of the elasticity of the silicone rubber lip, the effects of different values for the elasticity modulus are examined. In figure 5.3 the flow plots of different elasticity moduli are plotted. The $F0$ values and SPL values belonging to the different elasticity moduli are mentioned below the figure.

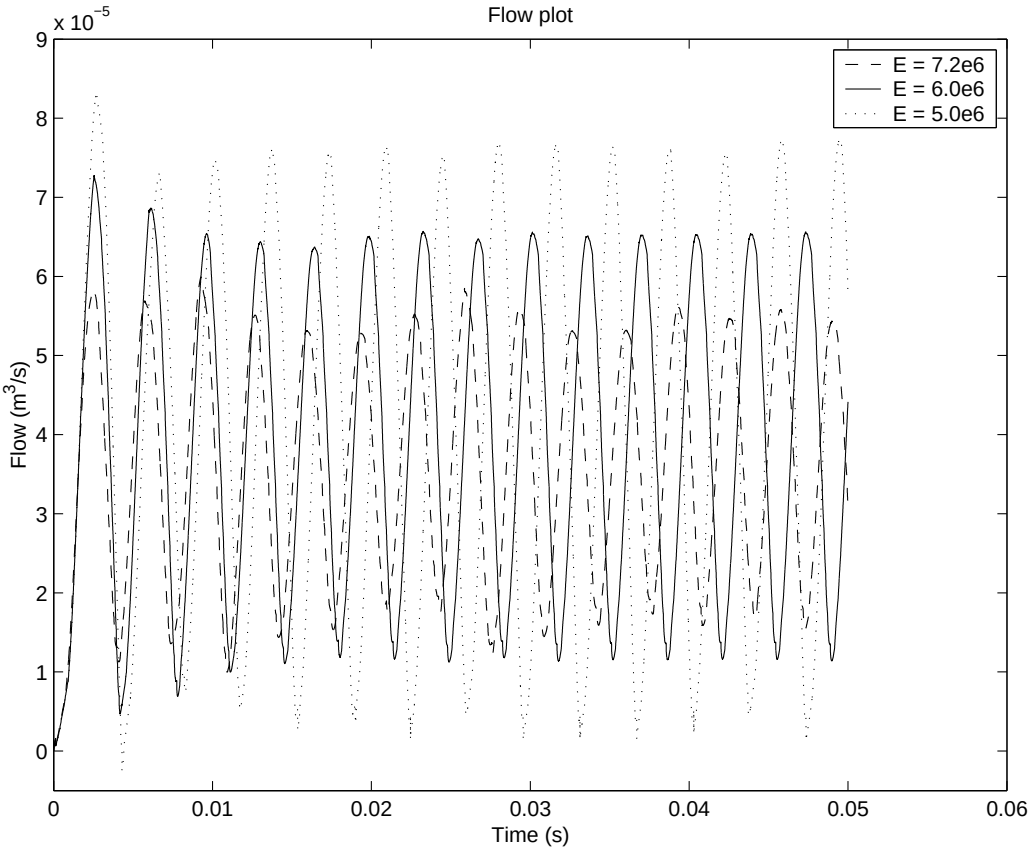

Figure 5.3: Flow plot comprising different values for the elasticity modulus

$E = 7.2 \cdot 10^6$ Pa

$F0 = 311$ Hz [7.0 %]	$SPL = 58$ dB [2.3 %]

$E = 6.0 \cdot 10^6$ Pa (standard simulation)

$F0 = 290$ Hz	$SPL = 59$ dB

$E = 5.0 \cdot 10^6\ Pa$

$F0 = 281\ Hz$ [3.2 %]	$SPL = 61\ dB$ [3.3 %]

Figure 5.3 shows various flow plots. A stiff lip (high elasticity modulus) results in smaller oscillations of the lip, i.e. a smaller maximum flow and a large minimum flow. A flexible lip (small elasticity modulus) results in larger oscillations of the lip, thus a larger maximum flow and a smaller minimum flow. Because of these larger movements of the lip, a refinement of the grid is necessary to assure a stable model. This can be seen in figure 5.3 by an oscillating flow which shows values below zero, which is remarkebly. Simulations which are performed with a lip with an elasticity modulus of $4.0 \cdot 10^6\ Pa$ or smaller will crash, because the movements of the lip will become too wild.

The elasticity modulus has a considerable influence on the $F0$ (percentages of about five percent). From the results it follows that the $F0$ decreases with the diminution of the elasticity modulus.

The influence of the elasticity modulus on the SPL is not really worth mentioning, since the SPL varies only less than 3 dB.

5.3 Pressure

In our computational model lip3D a silicone rubber lip moving in a rectangular housing is simulated (figure 1.4). To obtain oscillations of the lip a constant pressure, for example 500 Pa, is imposed at the beginning of the housing and a constant pressure of 0 Pa at the end of the housing. An increase of the prescribed pressure will result in bigger movements of the lip, i.e. the lip will reach a lower position in the housing so that the mean flow will increase.

To examine the exact influence of the pressure on the oscillations of the lip, simulations with different values for the prescribed pressure have been performed. In figure 5.4 the flow plots belonging to these simulations are shown. The corresponding $F0$ and SPL values are presented below.

$P = 1125\ Pa$

$F0 = 251\ Hz$ [13.7 %]	$SPL = 69\ dB$ [17.0 %]

$P = 750\ Pa$

$F0 = 233\ Hz$ [19.7 %]	$SPL = 66\ dB$ [12.8 %]

$P = 500\ Pa$ (standard simulation)

$F0 = 290\ Hz$	$SPL = 59\ dB$

$P = 333.33\ Pa$

$F0 = 285\ Hz$ [1.9 %]	$SPL = 49\ dB$ [16.5 %]

In figure 5.4 various flow plots can be seen. A high pressure results in a larger movement of the lip, i.e. a higher maximum flow, thus a higher mean flow, because the lip reaches a lower position in the housing. Similarly, a low pressure results in a smaller movement of the lip, i.e. a lower maximum flow, thus a lower mean flow. Because the model lip3D is very sensitive

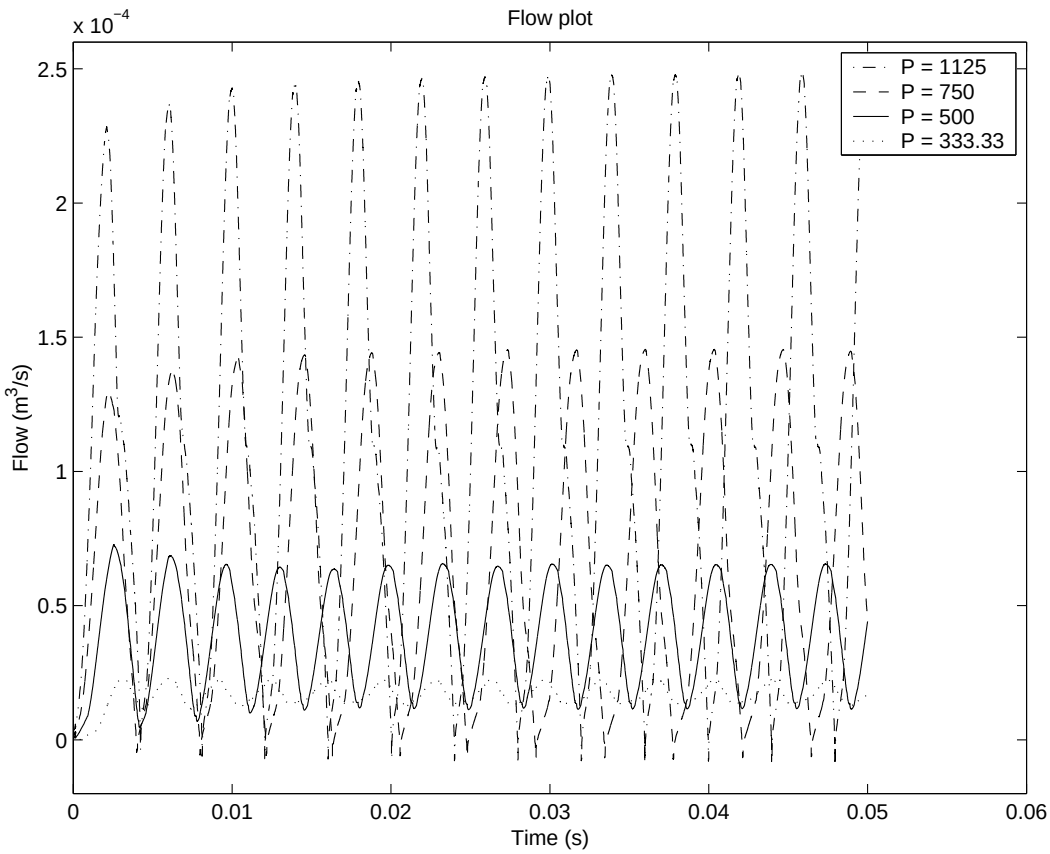

Figure 5.4: Flow plot comprising different values for the pressure

to large movements of the lip, grid refinement is necessary to assure a stable model if high pressure values are used. This can be seen in figure 5.4 by an oscillating flow which shows values below zero, which is remarkebly.

The pressure has a significant influence on the $F0$, since pressure values of 750 Pa and 1125 Pa result in an increase of the $F0$ of more than 10 percent. The relation between the pressure and the $F0$ is not very explicit. According to the values found in the simulation and since De Vries found an U-shaped relation between the pressure and the $F0$ (section 6.2), i.e. an unexpected decrease of the $F0$ by an increasing pressure, but when the pressure is increased further the $F0$ rises again, it is presumed that there is an U-shaped relation between the pressure and the $F0$.

The influence of the prescribed pressure on the SPL is big, since the SPL varies 7 dB and more. An increase of the pressure results in an increase of the SPL.

5.4 Number of dimensions

To achieve more realistic results and to investigate the influence of airflow along the sides of the silicone rubber lip a 3D numerical model is required. In the 2D standard simulation air was not able to flow along the sides of the lip. In a similar 3D simulation slits originate along the sides of the lip. As a result, the calculated minimal flow will become higher, because air is always able to flow along the sides of the lip.

In figure 5.5 the flow plots of the standard 2D simulation together with the similar 3D simulation are depicted. The values for the $F0$ and SPL belonging to the 2D and 3D simulation are mentioned below the figure.

grid = 96 x 1 x 30 cells (2D); 0.95 stretch in z-direction (standard simulation)

$F0 = 290\ Hz$	$SPL = 59\ dB$

grid = 96 x 26 x 30 cells (3D); 0.79846 stretch in y-direction, 0.95 stretch in z-direction

$F0 = 289\ Hz$ [0.6 %]	$SPL = 59\ dB$ [0.9 %]

The values for the $F0$ and SPL of the 2D and 3D simulation are approximately the same. As a result, the 2D and 3D simulations produce similar results, except for the flow, which differs significantly. Because of the slits along the side of the lip, air is always allowed to pass the lip. Therefore, the minimal flow becomes higher.

If the 3D simulation is run by the compiler f77 without optimization (section 4.1), incorrect results are produced, which can be seen in figure 5.6. This supports the usage of the compiler f77 with the compilation option -O.

5.4.1 Necessity of a 3D computational model

A 3D computational model has been developed, but we are still dealing with the question whether a third dimension is necessary, or that a 2D computational model would be sufficient.

In the previous section (section 5.4) it can be seen that adding a third dimension, so that air can flow along the sides of the lip, only influences the flow. But this possibility of flow along the sides of the lip has a negligible influence on the $F0$ or SPL.

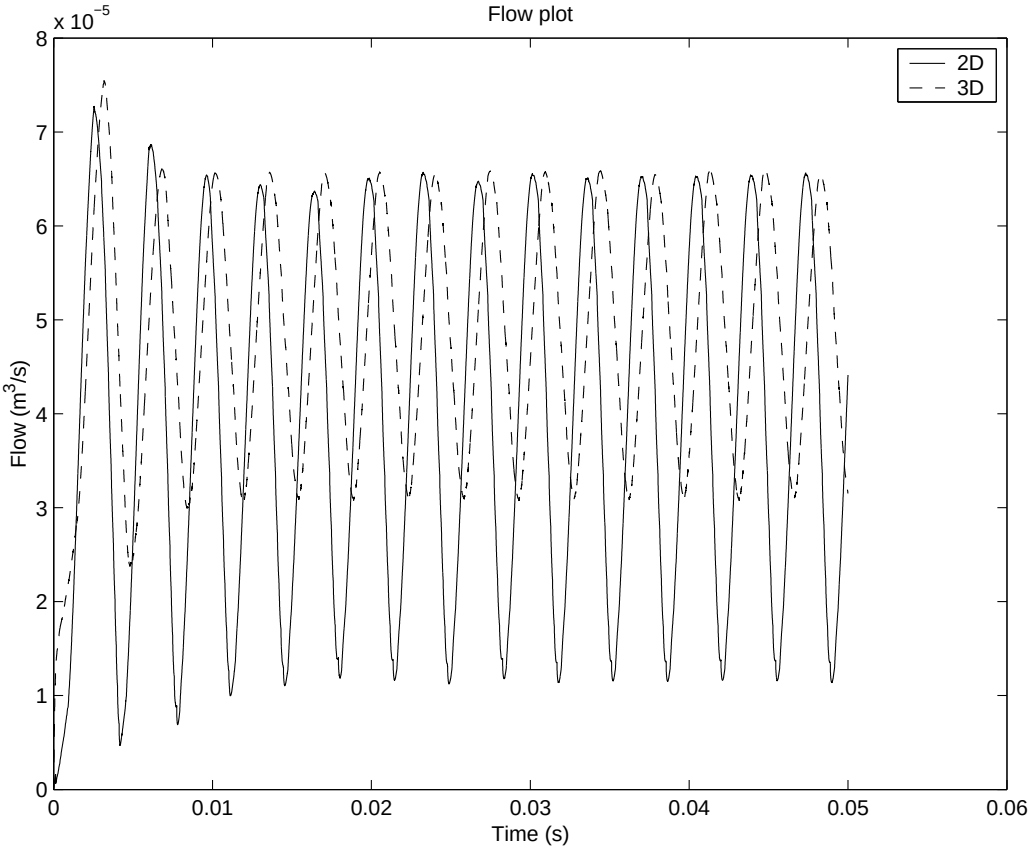

Figure 5.5: Flow plot comprising different dimensions

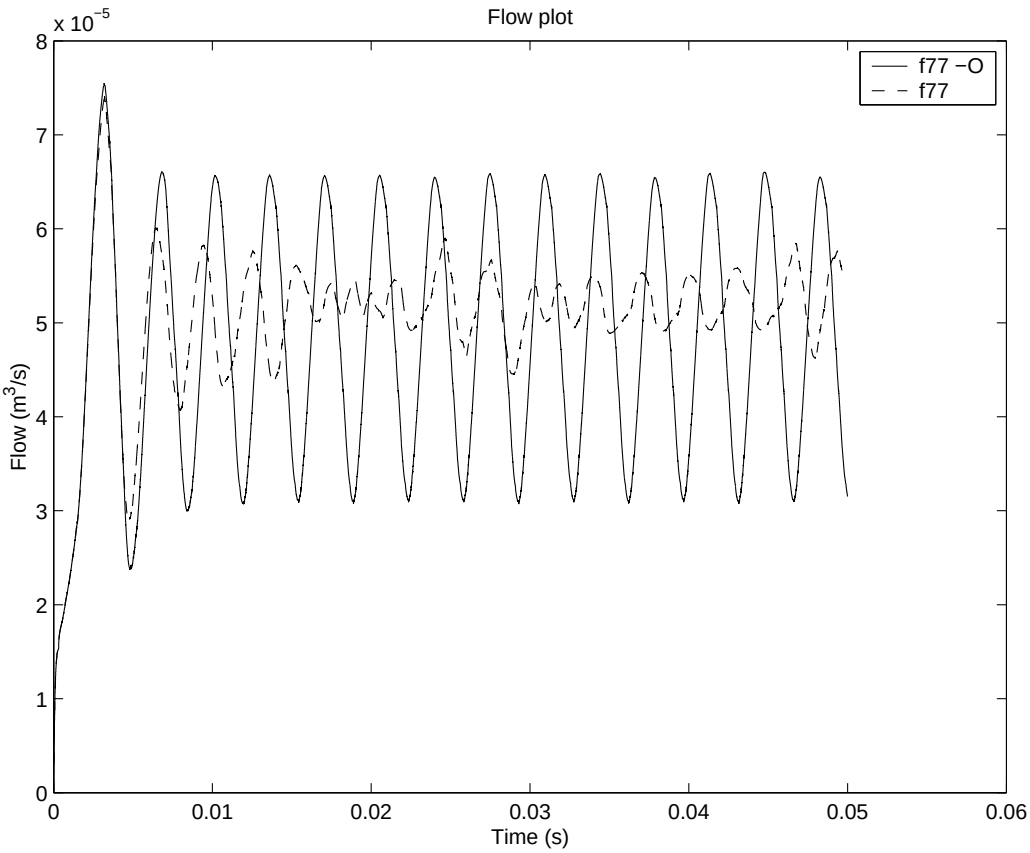

Figure 5.6: Flow plot comprising 3D simulations with different compiler options

To investigate the influence of the flow along the sides of the lip better, a closer look shall be taken to the lateral flow in front of the lip and behind the lip. Besides of the place of the lip, where the air can flow along the sides of the lip, there is no air flow in the lateral direction in front of the lip, as can be seen in figure 5.7. Behind the lip there is air flow in the lateral direction, but the velocities of this lateral flow are very small and since they apparently have a negligible influence on the $F0$ or SPL (section 5.4) they are insignificant.

So it can be concluded that in our situation, i.e. with simple movements of the lip in which the lowest position of the lip in the housing is halfway, there is no need for a third dimension. Therefore, a 2D computational model is sufficient. However, with bigger or wilder movements of the lip it first has to be checked whether the flow along the sides of the lip has a negligible influences the $F0$ or SPL, so that a 2D computational model can be used.

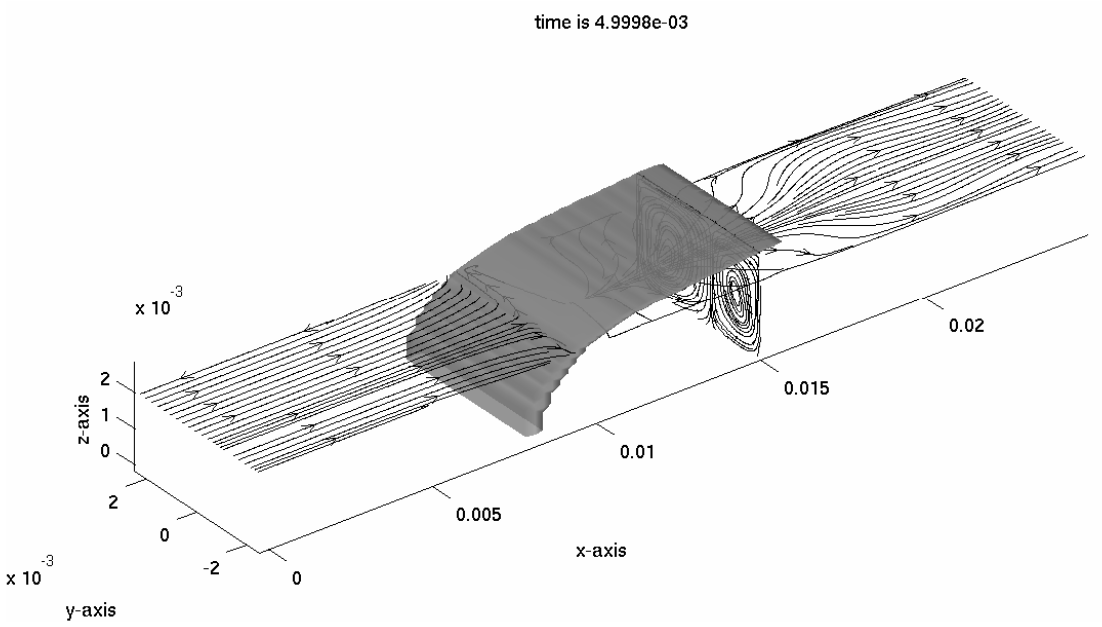

Figure 5.7: The air flow in the 3D computational model

5.5 Conclusions

To examine the performance of the computational model lip3D, the influence of different parameters have been investigated. The investigation of the influence of the damping coefficients c_{mass} and c_{stiff} showed that the influence of c_{mass} is negligible and that the influence of c_{stiff} is bigger, but still hardly worth mentioning. The elasticity modulus and the pressure both have a big influence on the behavior of the silicone rubber lip, especially on the flow and the $F0$. However, the pressure is the only parameter which has an enormous influence on the SPL. The investigation of the number of dimensions shows that the behavior of a 2D and 3D simulation are approximately the same, except that in a 3D model air is allowed to pass along the sides of the lip.

Except for the required grid refinement in simulations with a very flexible lip or with high

prescribed pressures, it can be concluded from the obtained results that the behavior of the model lip3D is reliable and seems to be realistic.

From the investigation in section 5.4.1 it is concluded that with simple movements of the lip, movements in which the lowest position of the lip is halfway the housing, a 2D computational model is sufficient. However, with bigger or wilder movements of the lip it first has to be verified whether air flow along the sides of the lip influences the $F0$ or SPL, so that a 3D computational model is necessary.

Chapter 6

Validation

6.1 In vitro experiments

To validate the results of the computational model lip3D in vitro experiments have been performed. In these experiments the pressure p, the fundamental frequency $F0$ and the sound pressure level SPL of a voice-producing element (figure 6.1) were measured at different airflows, ranging from $8 \cdot 10^{-5}$ till $30 \cdot 10^{-5}$ $\frac{m^3}{s}$. Thus instead of imposing a constant pressure at the beginning of the housing as in the computational model, a constant airflow was used.

Because of the movement of the silicone rubber lip, the pressure and flow in front of the lip oscillate. To realize a constant airflow at the beginning of the housing, the vpe was connected on top of a pressure vessel (figure 6.2). The function of the vessel was to neutralize the oscillations of the flow, originated by the oscillations of the lip. More information about the in vitro experiments can be found in the guide of the model lip3D [17].

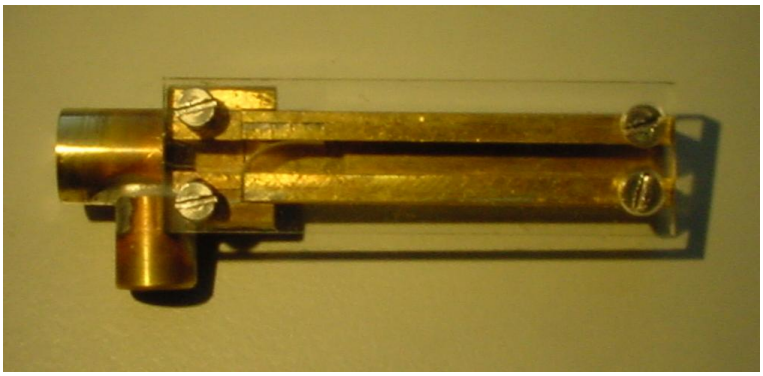

Figure 6.1: The vpe used in the in vitro experiments

There are a lot of differences between the setup of the in vitro experiments and the modelling of the vpe in the computational model lip3D. For example the width, height and elasticity modulus of the silicone rubber lip differ and in the computational model a constant pressure was imposed at the beginning of the housing of the vpe, instead of a realistic oscillating pressure. These differences will be discussed extensively in section 7.1. Because of these differences the results of the model lip3D and the in vitro experiments cannot be compared

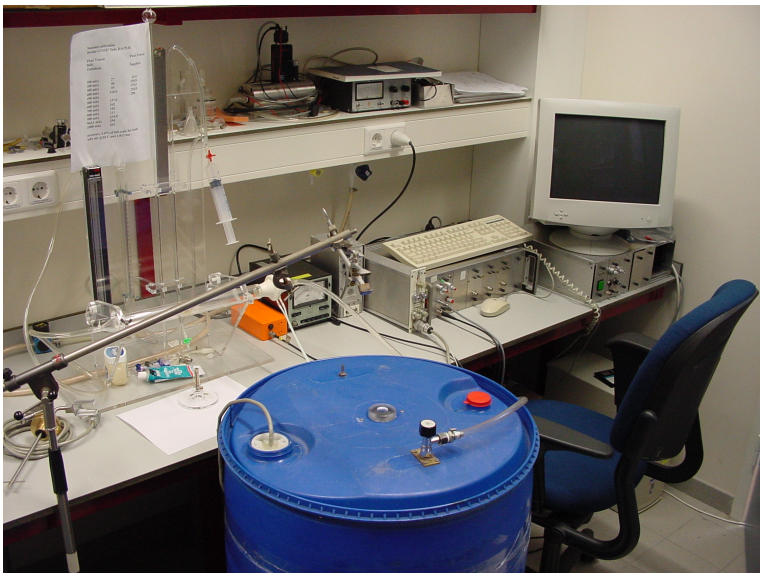

Figure 6.2: The setup of the in vitro experiments

p_{mean} (Pa)	Q_{mean} $(\frac{m^3}{s})$	$F0$ (Hz)	SPL (dB)
400	$8 \cdot 10^{-5}$	217	62
440	$10 \cdot 10^{-5}$	213	63
570	$15 \cdot 10^{-5}$	233	69
790	$20 \cdot 10^{-5}$	243	73
1160	$25 \cdot 10^{-5}$	292	76
1380	$30 \cdot 10^{-5}$	314	80

Table 6.1: In vitro results of 30/08/04

in detail. Therefore only attention will be paid to the results in general. The results of the in vitro experiments can be found in table 6.1.

The results of the in vitro experiments show the same general behavior of the silicone rubber lip as the results of the computational model lip3D (section 5.3). In both situations an increase of the pressure results in an increasing mean flow (and vice versa), and an increasing SPL. Moreover, both results show a presumed U-shaped relation between the pressure and the $F0$, i.e. an unexpected decrease of the $F0$ by an increasing pressure, but when the pressure is increased further the $F0$ rises again.

6.2 Earlier results

The results acquired by De Vries et al [8] showed the same general behavior of the voice-producing element. Numerical simulations of a vpe showed an increase of the mean flow as a result of an increasing pressure (and vice versa) and an U-shaped relation between the pressure and the $F0$. Also in their in vitro measurements an increase of the pressure resulted in an increasing mean flow (and vice versa) and an increasing SPL. Again an U-shaped relation between the pressure and $F0$ was found.

Chapter 7

Conclusions

After the development of the computational model lip3D, the results of the model have been verified and validated. Moreover, investigation has been done to the influence of different parameters. The verification, parameter study, including the necessity of a 3D computational model, and validation of the model lip3D are described in the previous three chapters.

In chapter 4 it is concluded after grid research and investigating the influence of ϵ, CFL-max, CFL-min and different compilers and additional options, that the computational model lip3D is numerically stable and that the results are numerically accurate.

In chapter 5 the influence of the damping coefficients c_{mass}, c_{stiff}, the elasticity modulus, the pressure and the number of dimensions were examined. From this parameter study and because the results obtained by the 2D computational model lip of Górska are similar to the 2D results obtaind by the 3D computational model lip3D (chapter 4), it follows that the results of the model lip3D are reliable and moreover, seem realistic.

Furthermore, in chapter 5 it is concluded that with simple movements of the lip, movements in which the lowest position of the lip is halfway the housing, a 2D computational model is sufficient. However, with bigger or wilder movements of the lip it first has to be verified whether air flow along the sides of the lip influences the $F0$ or SPL, so that a 3D computational model is necessary.

Finally, in chapter 6 in vitro experiments and earlier results confirm the reliability and the realism of the results, since both the in vitro experiments and the earlier results show the same general behavior of the voice-producing element.

It may be noticed that in this thesis no attention has been paid to the realization of the requirements concerning the sound of a vpe mentioned in section 1.2. This is, because in this stage of development of the computational model lip3D the main interest is the stability and realibility of the obtained results.

As a conclusion, our computational model lip3D is operational and the results are reliable and seem to be realistic. Still the model needs several improvements. In the next section these improvements will be discussed extensively.

7.1 Future work

The possible improvements of the model are numerous and of quite diverse nature. To keep a better overview they will be divided into two classes, namely numerical adjustments and physical adjustments. In the next sections we will discuss the deficiencies of our model and the adjustments that can be made to improve our model.

7.1.1 Numerical adjustments

Adaptive timesteps

As mentioned before (section 4.3), the computational model lip3D uses adaptive timesteps. If the fluid or structure is moving too wildly, i.e. the CFL number is too high, the current time step will be halved and the computation continues.

The model can be improved if, besides of the reduction of the current time step, the computations during this last time step would be recalculated by using this smaller time step instead of continuing the computation. As a result, the displacement of the lip would be restricted to at most one grid cell, and the computation error would become smaller.

Grid research

In this stage of development we are mainly interested in the stability and reliability of the obtained results (chapter 4) and the influence of several parameters (chapter 5). Therefore, the biggest priority is working with a stable grid. As a consequence, only little attention will be paid to smaller issues like the correct width of the lip, the precise position of the lip and the correct height of the fluid. The model lip3D can be improved after more grid research and removal of the flaws mentioned in the next paragraphs.

The actual width of the silicone rubber lip is 4.75 mm, whereas the lip in our computational model has a width of 4.77 mm, because of inattention during the search for a stable grid.

In standard position the silicone rubber lip of the vpe is pressed to the top of the housing. In our model there is a slit of one cell or more between the lip and the housing in the initial situation. After a few time steps the lip is pressed to the top of the housing.

In the model lip3D the height of the lip is represented by one cell. Therefore, the height of the housing has no meaning and we will instead look at the amount of fluid over which the lip is able to move. It may be noticed that this amount of fluid changes during the computation since the lip oscillates and a nonuniform grid is used, namely a grid with stretch in the z-direction. In the initial situation the amount of fluid in our model is 2.803 mm instead of the actual amount of 2.744 mm (not including the cases of grid refinement).

As mentioned above, our model uses a grid with stretch in the z-direction, i.e. a fine grid at the top of the housing and consequently a coarse grid at the bottom of the housing. If during its oscillations the lip starts colliding with the lower wall, it might be important that there is a fine grid at both the top and bottom of the housing. Because of the computation time the grid only has a fine grid at the top of the housing. To improve the model more research has to be done to collisions with the lower wall.

Post-processing

The post-processing part of lip3D is primarily used to visualize the obtained results. At the moment the post-processing part in lip3D is placed between the fluid and structure part. The model can be improved by moving the post-processing part to the end of the cycle, namely below the fluid part. This way the post-processing data will contain fluid and structure information of the same time step, instead of structure information of the previous time step.

Spectra

If the elasticity modulus of the silicone rubber lip or the prescribed pressure at the beginning of the housing of the vpe increases, the movements of the lip become larger. Because the model is very sensitive to large movements of the lip, refinement of the grid is necessary to assure a stable model. This can be seen in figure 5.3 and 5.4 by an oscillating flow which shows values below zero (which is physically rather unlikely).

In this thesis no attention has been paid to spectrum plots. The reason is that first more research has to be done to the cause of the origin of harmonics in the spectrum plots. For example, if the prescribed pressure is increased more harmonics originate in the spectrum plot. This is realistic, but these harmonics may also arise because of the flow values below zero, which are a result of insufficient grid refinement.

Since examining the spectrum plots is desirable, so that the results of the computational model can be investigated better and more detailed, first more research has to be done to the cause of the origin of harmonics in the spectrum plots.

7.1.2 Physical adjustments

Elasticity modulus

In section 5.2 is explained that the computation model lip3D uses a silicone rubber lip with an elasticity modulus of $6.0 \cdot 10^6$ Pa, instead of a realistic value between $1.3 \cdot 10^6$ and $4.0 \cdot 10^6$ Pa, to assure the stability of the model. The model can be improved by taking care that the model can handle lips with lower elasticity moduli, such as $4.0 \cdot 10^6$ Pa, as well.

Moreover, our computational model with a silicone rubber lip of $E = 6.0 \cdot 10^6$ Pa uses an inputfile bendflap.txt corresponding to $E = 3.5 \cdot 10^6$ Pa. As a result, the initial load on the lip will be too low. This is physically not correct, but it results in a stable model, which is our main purpose, so that the stability and reliability of the obtained results and the influence of several parameters can be investigated. It would be an improvement if the model and the inputfiles would use the same elasticity modulus.

Damping coefficients

As mentioned in section 5.1, De Vries and Hamburg adjusted the values for the damping coefficients c_{mass} and c_{stiff} of the silicone rubber to match the results of the in vitro experiments, because they could find no information in the literature.

As a result, the obtained results are not very reliable. It would be an improvement of the model if the values of the damping coefficients would be determined by a damping experiment, so

that the results of our computational model can be better tested by the in vitro experiments. In our case the damping experiment is the investigation of the degree of damping of a vibrating lip of silicone rubber that is held on both ends. Comparable experiments are done for the determination of the damping coefficients of wings by the National Aerospace Laboratory NLR.

Pressure

In the computational model lip3D oscillations of the lip are obtained by imposing a constant pressure, for example 500 Pa, at the beginning of the housing and a constant pressure of 0 Pa at the end of the housing. However, in vitro experiments showed that at the beginning of the housing the pressure was not constant as claimed, but fluctuated because of the movement of the lip.

Therefore, the determination of a place with a constant pressure was preferred. In vitro experiments showed that 3.25 mm in front of the housing, the pressure fluctuated only 5% (thus a pressure of 500 Pa was allowed to vary from 475 till 525 Pa) [17].

To obtain a physically correct computational model the same oscillating pressure, as found in the in vitro experiments, has to be imposed at the beginning of the housing or this extra 3.25 mm has to be implemented in the geometry.

The development of a second computational model lip3D_chamber, in which this extra 3.25 mm is implemented, has started, but more grid research is necessary to obtain a stable model. Moreover, it has to be investigated whether the model uses the values of the top and bottom of the housing given by the user or the corresponding values of the grid, since in this new model these values differ [17].

Modelling of the lip

As mentioned before, the height of the silicone rubber lip in our model is represented by one cell instead of the actual height of 0.266 mm. Since a nonuniform grid is used, the height of the lip varies during the simulation of our model, because of the oscillations of the lip.

The model lip3D can be improved if the lip is represented by more cells and has a practically constant height corresponding to the actual height of the lip. Consequently, the results would become more realistic and a better grid research (section 4.4) and research to the influence of the height of the lip could be done.

7.1.3 Lower priority adjustments

More adjustments can be made to improve the performance of the model. The deficiencies and adjustments of the model mentioned below have a lower priority than the one mentioned in the previous sections.

Number of lip elements

At the moment the model lip3D uses a lip consisting of twelve beam elements (figure 3.3). The thirteen nodes are uniformly divided over the lip, independent of the curvature of the lip. The model can be improved if locally more nodes are used at the positions of the lip with the largest curvature. E.g. more elements are locally needed to simulate the curvature of the lip around node 2 (figure 3.4).

3D elastic equation

In our model the silicone rubber lip is described by the 2D elastic equation (3.5). To obtain a 3D lip a third dimension, namely a constant width, is added. This means that still no torsion of the lip is possible. Therefore, the model can be improved by developing a new 3D elastic equation for the silicone rubber lip, so that torsion of the lip is possible.

Predictor-corrector algorithm

The 3D computational model of the vpe is solved numerically with a loose coupling algorithm (section A.2.4). It would be an improvement of the model lip3D if, instead of the loose coupling algorithm, the predictor-corrector algorithm (section A.2.4) would be used.

A disadvantage of using the predictor-corrector algorithm is that it will cost a lot of development time. By using the predictor-corrector algorithm internal iterations are used, meaning that it waits for the fluid-structure interaction to converge. Therefore, the advantage of using the predictor-corrector algorithm is that the results will become more accurate. As a consequence bigger time steps are possible and less computing time is needed.

Extension to various geometries

As mentioned in section 7.1.2 the development of a second 3D computational model has started to simulate a different geometry. It would be an improvement if only one 3D computational model was developed that can handle different geometries. This way the model would become more user-friendly.

Appendix A

Coupled problems

The mathematical definition of a coupled problem according to Zienkiewicz [6] reads:

> "A coupled problem is a problem with bidirectional interactions of (usually different) physical effects without any possiblilty of an independent solution of a subproblem on its respective domain."

In other words, a coupled problem is a problem consisting of different subproblems, defined on different (possibly coinciding) domains, but which cannot be solved independently.

Coupled problems are applied in many fields of science, but in this paper we concentrate on fluid-structure interaction (FSI) problems.

A.1 Classification of coupled problems

There are many coupled problems. To keep an overview, these problems can be divided in different classes. There are several ways to classify the coupled problems. Classification may be based on the following.

A.1.1 Strong and weak

To be precise, these terms indicate the strength of the interaction between the subproblems, concerning the coupled problem. This classification is used often, but it is not a good one, because of multiple reasons. For example there exists no clear boundary between the classes strong and weak. Besides the degree of interaction is not known at the beginning [9].

A.1.2 Extent

According to this principle, the coupled problems can be divided in two classes, those with totally or partially overlapping domains and those with non-overlapping domains [6, 9].

The problems with totally or partially overlapping domains are coupled via differential equations that, usually, refer to different underlying physical phenomena. Thermal-magnetic problems are an example of this class.

With non-overlapping domains coupling occurs at the domain interfaces, i.e. via boundary conditions. This class can be divided further in two subclasses, problems with identical

physics and variables, such as the interaction between a structure and another structure, and problems with different underlying physics or different variables. Our problem, a FSI problem, is an example of this latter class.

A.1.3 Discretization method

Partial differential equations are very important in applied mathematics and engineering, since many real physical situations can be modelled by them. To solve these equations numerically, discretization methods are used, such as the finite volume method, the finite element method, the finite difference method or the boundary element method (also called boundary integral method) [2, 25].

With this principle coupled problems can be divided in two groups. The first group is called homogeneous, which means that all subproblems of the coupled problem use the same discretization method. The other group is called hybrid, i.e. the subproblems use different discretization methods [9].

Our mathematical problem belongs to the hybrid group, that means we will use a different discretization method for the silicone lip than the one used for the airflow. This is correct since we will solve the lip by a finite element method and the airflow by a finite volume method.

A.1.4 Global non-linear numerical solution algorithm

The fourth and most interesting division of the coupled problems is based on the way the problems are solved. We distinguish two solution algorithms, namely a monolithic coupling scheme and a partitioned coupling scheme [6, 9, 22]. These solution algorithms and other methods to solve coupled problems will be explained in the next section.

A.2 Solving coupled problems

Because there are so many different coupled problems, there is no general approach to solve coupled problems. There are many methods to solve a coupled problem. These methods can be separated in different divisions and subdivisions, which all have their advantages and disadvantages. In this section these methods will be discussed. It has to be mentioned that this overview might not be complete, but it covers the main part.

A.2.1 Monolithic and partitioned coupling scheme

The first division of methods to solve coupled problems is based on the manner the subproblems are coupled. As was mentioned in the previous section, there are two classes of coupling schemes, the monolithic coupling scheme and the partitioned coupling scheme [6, 22].

Monolithic coupling scheme

Monolithic coupling schemes are also known as simultaneous coupling schemes or fully coupled algorithms. With this coupling scheme the subproblems are coupled first, after which the coupled problem is solved in one step.

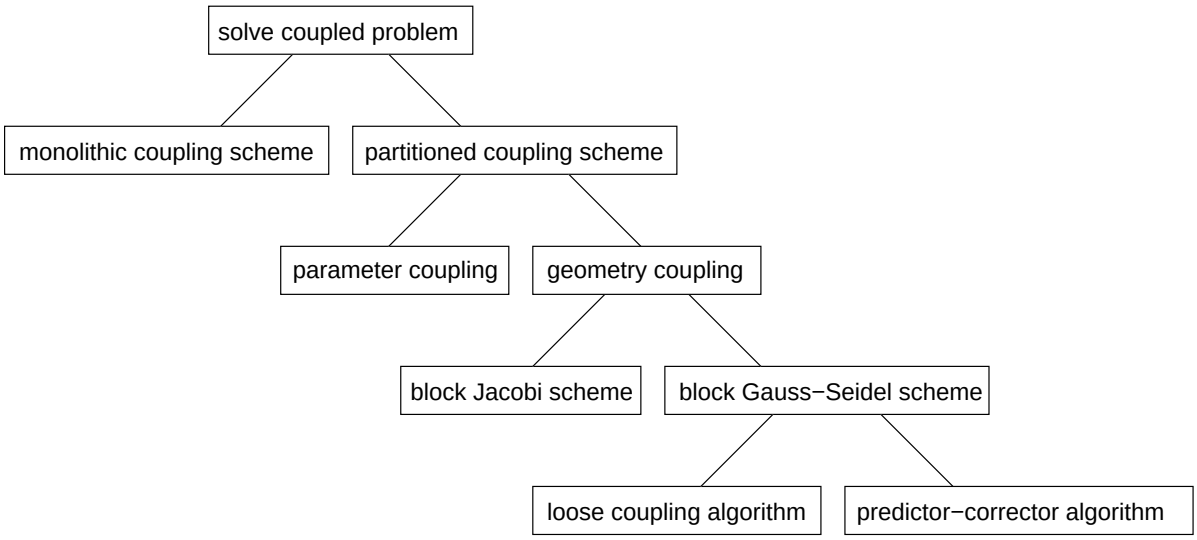

Figure A.1: Scheme of solving a coupled problem

The advantage of this method is that it is more robust than methods based on iterations, like the partitioned coupling scheme. For instance it does not suffer the consequences of iterations, such as the possibility of divergence. But this method also has many disadvantages [6, 26]. For example it requires a lot of memory and computational time. Moreover, a total new single program has to be developed instead of making use of existing code. Furthermore, the algebraic equations of the coupled problem can be too stiff, because the equations of the fluid mechanics and structural mechanics often differ significantly from each other.

An example of a monolithic coupling scheme is found in the paper written by Iemma and Pontrelli [19], in which they examine a blood-vessel system.

Partitioned coupling scheme

With a partitioned coupling scheme, also named a staggered scheme or internal cascade algorithm, the subproblems are solved separately and an outer iteration is used for coupling the subproblems.

The first advantage of this method is the possibility to make use of existing code to solve the individual subproblems, with only minor adjustments necessary. Additionally this coupling scheme is very flexible concerning the problems to be solved and code to be used. E.g. the link of two different numerical discretization methods, such as the link of a finite element model of the structure to a finite volume model of the surrounding fluid. So it allows independent use of suitable discretization methods for the individual subproblems. And apart from that it requires relatively small amounts of memory [6, 10, 26].

One should be aware that attention must be paid to the numerical stability and accuracy of the model, since these may be affected by a partitioned treatment [10].

A.2.2 Parameter and geometry coupling

Partitioned coupling schemes are subdivided in two coupling methods, parameter coupling and geometry coupling [6].

Parameter coupling

With parameter coupling the coupling equations, which link the subproblems, combine the subproblem variables and the coupling parameters. An application of this coupling method is seen in thermo-mechanical problems.

Geometry coupling

In contrast, with geometry coupling the coupling equations combine the subproblems variables and changes in the underlying geometry. This principle is found in e.g. fluid-structure interaction.

A.2.3 Block Jacobi and block Gauss-Seidel scheme

Geometry coupling can be divided further by investigating different iterative solvers. Two methods will be mentioned here, the block Jacobi scheme and the block Gauss-Seidel scheme [6].

Block Jacobi scheme

A block Jacobi scheme regards a concurrent solution of the subproblems. The subproblems are first solved parallel, after which data can be exchanged (figure A.2).

This method requires a considerable amount of storage and does not make use of the newest information available. Besides these disadvantages the convergence is not guaranteed or is often too slow [20, 21].

Block Gauss-Seidel scheme

Unlike a block Jacobi scheme, a block Gauss-Seidel scheme concerns an alternate solution of the subproblems, i.e. the subproblems are solved alternately and in between the data is exchanged (figure A.3).

The drawbacks of this method are also seen with the block Jacobi scheme. There is no guarantee that the method will converge and if it converges it is often too slow [21].

However the block Gauss-Seidel scheme does use the updated values as soon as they are available. As a result of this the block Gauss-Seidel scheme uses half the storage the block Jacobi method uses, because there is no need to maintain the old values. Finally this method converges faster [20].

A.2.4 Loose coupling and predictor-corrector algorithm

As a last division the block Gauss-Seidel scheme can be divided into two groups, by the difference in time stepping scheme [22].

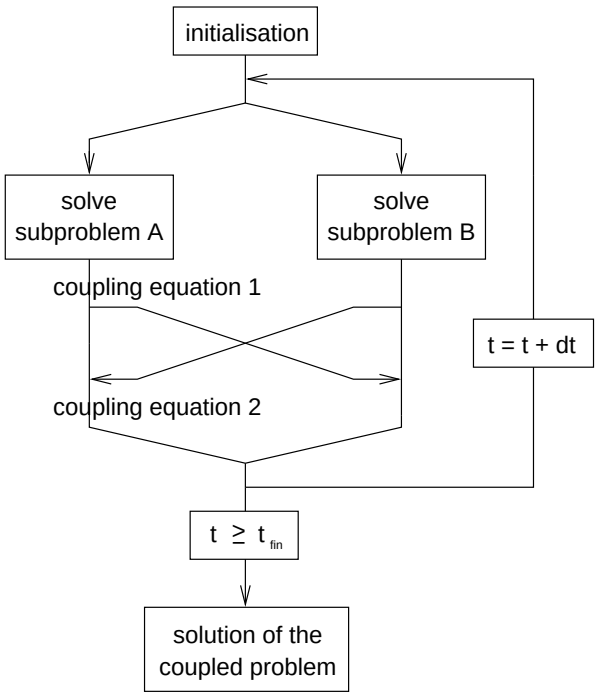

Figure A.2: A schematic representation of the block Jacobi scheme

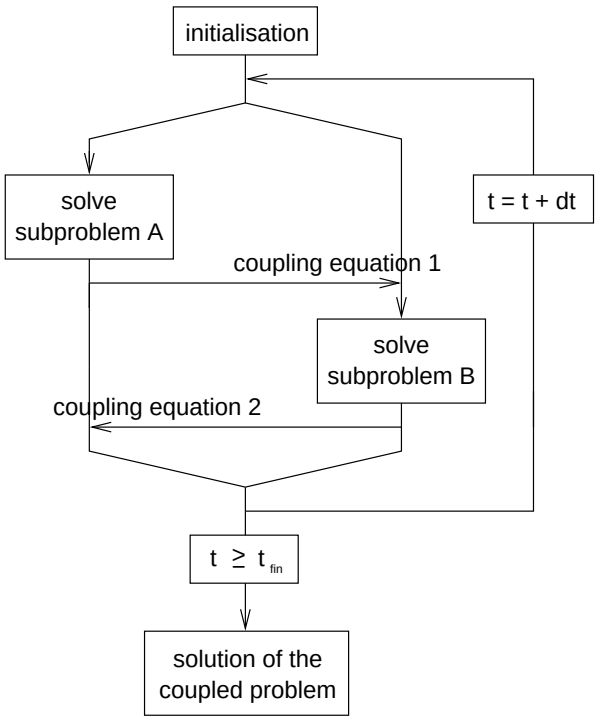

Figure A.3: A schematic representation of the block Gauss-Seidel scheme

Loose coupling algorithm

The first time stepping scheme is the loose coupling of the subproblems, such as the structural part and the fluid part. With this method only once per time step an interaction of the subproblems occurs.

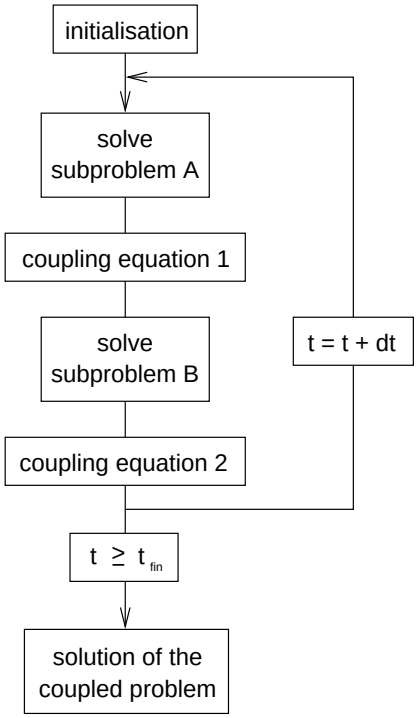

Figure A.4: A schematic representation of the loose coupling algorithm

Although this approach is rather easy to program and practical to start solving the coupled problem with, it has several disadvantages [22]. To start with a loose coupling method does not make use of internal iterations, meaning that it does not wait for the fluid-structure interaction to converge. Therefore errors arise and loss of order of accuracy occurs. Consequently no big time steps are possible, so there is a limitation of the feasible time step.

The loose coupling algorithm is used very often. Examples are the simulation of an artifical aortic valve [24], the simulation of a micropump [6] and the interaction of a thin-walled structure with a fluid [39]. Moreover, we will use a loose coupling algorithm to solve our FSI problem.

Predictor-corrector algorithm

The second time stepping scheme is a predictor-corrector algorithm. After an initial predictor step, corrector steps are taken until convergence of the FSI is reached, after which time incrementation occurs and the process will be repeated. I.e. per time step the algorithm will be repeated until convergence occurs.

Due to the internal iterations smaller errors are produced and the loss of order of accuracy is reduced. This means that with the same time step better results are obtained, than when

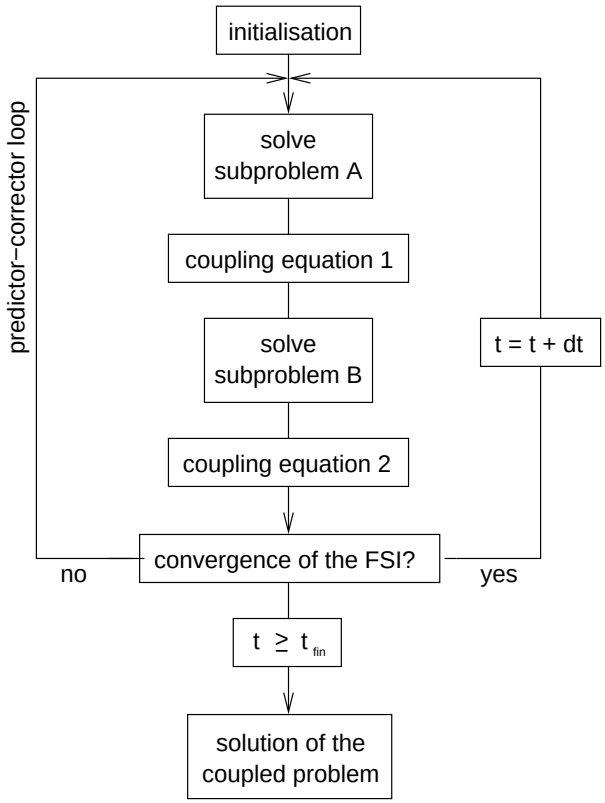

Figure A.5: A schematic representation of the predictor-corrector algorithm

the predictor-corrector algorithm is used. Moreover, because of this reduction of the loss of accuracy, bigger time steps are applicable. Another consequence of the internal iteration is that a noticeable reduction of the overall computing time can be achieved [22].

The application of a predictor-corrector algorithm is found in the paper written by Riemslagh et al. [28], concerning the interaction between a fluid and a flexible wall. In the paper written by Meynen et al. [22], they compare the results of a simple FSI problem obtained by using a loose coupling algorithm, with the results obtained by using a predictor-corrector algorithm.

Bibliography

[1] *Cray sv1e.* Internet, Centre for High Performance Computing & Visualisation, University of Groningen. (`http://www.rug.nl/rc/hpcv/computing/cray`)

[2] *Partial differential equations.* Internet. (`http://www.soundsoft.demon.co.uk/appmath/pde.htm`)

[3] *Patient information. Laryngectomy.* Internet, The Royal Marsden Hospital. (`http://www.royalmarsden.org/patientinfo/booklets/laryngectomy/index.asp`)

[4] E. F. F. Botta, *Eindige-Differentiemethoden*, Department of Mathematics, University of Groningen, November 1998.

[5] E. F. F. Botta, *De Methode der Eindige Elementen*, Department of Mathematics, University of Groningen, November 1999.

[6] H. Bungartz, A. Frank, F. Meier, T. Neunhoeffer, and S. Schulte, *Fluid structure interaction: 3D numerical simulation and visualization of a micropump*, Institut für Informatik der Technischen Universität München, April 1997. (`http://wwwzenger.informatik.tu-muenchen.de/persons/neunhoef/pumpe.ps.gz`)

[7] R. W. Clough and J. Penzien, *Dynamics of Structures*, McGraw-Hill, Inc., 1975.

[8] M. P. de Vries, *A new voice for the voiceless. Design and in-vitro testing of a voice-producing element*, PhD thesis, Faculty of Medical Sciences, University of Groningen, 2000. (`http://www.ub.rug.nl/eldoc/dis/medicine/m.p.de.vries/`)

[9] J. Driesen, *Coupled Electromagnetic-Thermal Problems in Electrical Energy Transducers*, PhD thesis, Department Electrical Engineering (ESAT), Catholic University of Leuven, May 2000. (`http://www.esat.kuleuven.ac.be/~driesen/work/doct/texts/PhD_JD.pdf`)

[10] C. Farhat, *Coupled field problems.* Internet, Center for Aerospace Structures, University of Colorado at Boulder. (`http://caswww.colorado.edu/~charbel/CFields.html`)

[11] G. Fekken, *Numerical simulation of greenwater loading on the foredeck of a ship*, Master's thesis, Department of Mathematics, University of Groningen, August 1998.

[12] A. A. Geertsema, *Tracheostoma valves and their fixation : towards an artificial larynx*, PhD thesis, Faculty of Medical Sciences, University of Groningen, 2000. (`http://www.ub.rug.nl/eldoc/dis/medicine/a.a.geertsema/`)

[13] J. Gerrits, *Dynamics of Liquid-Filled Spacecraft. Numerical Simulation of Coupled Solid-Liquid Dynamics*, PhD thesis, Department of Mathematics, University of Groningen, December 2001. (http://www.ub.rug.nl/eldoc/dis/science/j.gerrits/)

[14] M. Górska, *Numerical modelling of a voice-producing element*, Master's thesis, Department of Mathematics, University of Groningen, December 2002.

[15] W. Grolman, *Voice rehabilitation after total laryngectomy.* Internet, May 2000. (http://www.orl.nl/laryngectomy/)

[16] M. C. Hamburg, *Development of a numerical model of a voice producing element using the finite element method in combination with Navier-Stokes equations*, Master's thesis, Faculty of Mechanical Engineering, University of Twente, October 1999.

[17] M. M. Hegeman, *Guide to the 3D numerical model lip3D.f*, March 2004. (http://www.fmf.nl/~nonnie/Afstuderen/handleiding.html)

[18] I. Hočevar-Boltežar and M. Žargi, *Communication after laryngectomy*, Radiology and Oncology, 35(4) (2001), pp. 249–254. (http://www.onko-i.si/radiolog/013504/hocevar.pdf)

[19] U. Iemma and G. Pontrelli, *A boundary integral equation approach for fluid-wall interaction in arterial vessels*, in BIOFLUMEN Biological Fluid Mechanics Network. Abstract book, M. Grigioni and G. Pedrizzetti, eds., ISTISAN Congressi, Rome, April 2002, Istituto Superiore di Sanità, pp. 59–63. (http://www.iss.it/publ/cong/2002/02C1.pdf)

[20] R. Jenkins, *Assessing random iteration: A study examining parallel iterative solvers*, Master's thesis, The Department of Mathematics, The University of Southern Mississippi, February 2002. (http://pax.st.usm.edu/kolibal/ugr_html/jenkins_html/THESISc.pdf)

[21] H. G. Matthies and J. Steindorf, *Fully coupled fluid-structure interaction using weak coupling*, in Proceedings in Applied Mathematics and Mechanics, vol. 1, Zürich, 2001, Gesellschaft für Angewandte Mathematik und Mechanik (GAMM). (http://www.wire.tu-bs.de/OLDWEB/steindorf/gamm2001.ps.gz)

[22] S. Meynen, J. Mayer, and M. Schäfer, *Coupling algorithms for the numerical simulation of fluid-structure-interaction problems*, in ECCOMAS 2000 Proceedings (CD-ROM), Barcelona, September 2000, European Community on Computational Methods in Applied Sciences and Engineering (ECCOMAS).

[23] C. Mitchell and E. Moretz, *Speech options for laryngectomy patients.* Internet, University of North Carolina at Chapel Hill, May 2000. (http://www.unc.edu/~chooper/classes/voice/webtherapy/laryngectomy/speechoptions.html)

[24] V. Moreau, *Simulation 2d of the closure of an artificial aortic valve by blood reflux using arbitrary lagrangian eulerian (ale) formulation.* Internet, Center for Advanced Studies, Research and Development in Sardinia (C.R.S. 4), July 1997. (http://www.crs4.it/~moreau/PreEa/Papers/valvola.ps.gz)

[25] G. Morgenthal, *Comparison of numerical methods for bridge-deck aerodynamics*, Master's thesis, Magdalene College, University of Cambridge, August 2000. (`http://www2.eng.cam.ac.uk/~gm249/gm_MPhil.pdf`)

[26] M. A. Perlz, *FIDAP 8.5 Documentation*, Fluent incorporated, update manual ed., July 1999. Chapter 3, section 3.2.1. (`http://www.unc.edu/atn/asg/applications/fluent/fidap8.7.2/documentation/html/f85/f85toc.htm`)

[27] R. L. Plant, *The voice center. Laryngeal cancer: Index.* Internet, The Voice Center, Eastern Virginia Medical School, October 2002. (`http://www.voice-center.com/laca_index.html`)

[28] K. Riemslagh, V. Vierendeels, and E. Dick, *An efficient coupling procedure for flexible wall fluid-structure interaction*, in ECCOMAS 2000 Proceedings (CD-ROM), Barcelona, September 2000, European Community on Computational Methods in Applied Sciences and Engineering. (`http://www.csc.fi/elmer/papers/eccomas2001_raback.pdf`)

[29] H. K. Schutte. Personal communication, November 2002.

[30] H. K. Schutte. Personal communication, December 2003.

[31] J. P. Searl and L. H. Small, *Acoustic correlates of gender in tracheoesophageal speech.* Internet, Department of Communication Disorders, Bowling Green State University, 2001. (`http://www.bgsu.edu/departments/cdis/cdis_content/resources/pdf/Searl1.pdf`)

[32] A. van der Ploeg, *Preconditioning for sparse matrices with applications*, PhD thesis, Department of Mathematics, University of Groningen, 1994.

[33] M. van der Torn, M. P. de Vries, J. M. Festen, I. M. V. de Leeuw, and H. F. Mahieu, *Alternative voice after laryngectomy using a sound-producing voice prosthesis*, The Laryngoscope, 111(2) (2001), pp. 336–346. (`http://web.inter.nl.net/users/vanderTorn/Med/Laryngoscope_Febr2001/Laryngoscope_Febr2001.html`)

[34] M. van der Torn, H. F. Mahieu, and J. M. Festen, *Aero-acoustics of silicone rubber lip reeds for alternative voice production in laryngectomees*, The Journal of the Acoustical Society of America, 110(5) (2001), pp. 2548–2559. (`http://web.inter.nl.net/users/vanderTorn/Med/JASA_Nov2001/JASA_Nov2001.pdf`)

[35] A. E. P. Veldman, *Computational Fluid Dynamics*, Department of Mathematics, University of Groningen, September 2001.

[36] A. E. P. Veldman. Personal communication, November 2003.

[37] G. J. Verkerke. Personal communication, December 2002.

[38] G. J. Verkerke. Personal communication, March 2004.

[39] W. A. Wall and E. Ramm, *A coupled fluid structure environment with a three-dimensional shell model*, in ECCOMAS 2000 Proceedings (CD-ROM), Barcelona, September 2000, European Community on Computational Methods in Applied Sciences and Engineering (ECCOMAS).